BNL-93903-2010

Neutron Cross section Covariances in the Resonance region: ^{52}Cr, ^{56}Fe, ^{58}Ni

P.Oblozinsky, Y.-S.Cho[*)], C.M.Mattoon, S.F.Mughabghab

National Nuclear Data Center, Brookhaven National Laboratory

Upton, NY 11793- 5000, USA

*) On sabbatical leave from Nuclear Data Laboratory, KAERI, Korea

Final version: August 3, 2010

National Nuclear Data Center
Brookhaven National Laboratory
P.O. Box 5000
Upton, NY 11973-5000
www.nndc.bnl.gov

Notice: This manuscript has been authored by employees of Brookhaven Science Associates, LLC under Contract No. DE-AC02-98CH10886 with the U.S. Department of Energy. The publisher by accepting the manuscript for publication acknowledges that the United States Government retains a non-exclusive, paid-up, irrevocable, world-wide license to publish or reproduce the published form of this manuscript, or allow others to do so, for United States Government purposes.

DISCLAIMER

This report was prepared as an account of work sponsored by an agency of the United States Government. Neither the United States Government nor any agency thereof, nor any of their employees, nor any of their contractors, subcontractors, or their employees, makes any warranty, express or implied, or assumes any legal liability or responsibility for the accuracy, completeness, or any third party's use or the results of such use of any information, apparatus, product, or process disclosed, or represents that its use would not infringe privately owned rights. Reference herein to any specific commercial product, process, or service by trade name, trademark, manufacturer, or otherwise, does not necessarily constitute or imply its endorsement, recommendation, or favoring by the United States Government or any agency thereof or its contractors or subcontractors. The views and opinions of authors expressed herein do not necessarily state or reflect those of the United States Government or any agency thereof..

Neutron cross section covariances in the resonance region: ^{52}Cr, ^{56}Fe, ^{58}Ni

P. Obložinský, Y.-S. Cho*), C.M. Mattoon, S.F. Mughabghab

National Nuclear Data Center, Brookhaven National Laboratory
Upton, New York, 11973 – 5000, U.S.A.

*) On sabbatical leave from Nuclear Data Laboratory, KAERI, Korea

Final version: August 3, 2010

Notice: This manuscript has been authored by employees of Brookhaven Science Associates, LLC under Contract No. DE-AC02-98CH10886 with the U.S. Department of Energy. The publisher by accepting the manuscript for publication acknowledges that the United States Government retains a non-exclusive, paid-up, irrevocable, world-wide license to publish or reproduce the published form of this manuscript, or allow others to do so, for United States Government purposes.

Abstract

We evaluated covariances for neutron capture and elastic scattering cross sections on major strucutral materials, ^{52}Cr, ^{56}Fe and ^{58}Ni, in the resonance region which extends beyond 800 keV for each of them. Use was made of the recently developed covariance formalism based on kernel approximation along with data in the Atlas of Neutron Resonances. The data of most interest for AFCI applications, elastic scattering cross section uncertainties at energies above about few hundred keV, are on the level of about 12% for ^{52}Cr, 7-8% for ^{56}Fe and 5-6% for ^{58}Ni.

Contents

1 Introduction **2**

2 Evaluation procedure **4**
2.1 Radiative capture 4
2.1.1 Thermal region 4
2.1.2 Average cross sections in the resonance region 5
2.1.3 Uncertainties in the resonance region 7
2.1.4 Covariance matrix 8
2.2 Elastic scattering 9
2.2.1 Thermal region 9
2.2.2 Average cross sections in the resonance region 9
2.2.3 External resonances 11
2.2.4 Uncertainty for a single resonance 14
2.2.5 Uncertainty for many resonances 16
2.2.6 Correlation coefficients 17
2.2.7 Covariance matrix 18

3 Evaluations **19**
3.1 Preparatory analysis 19
3.1.1 List of materials 19
3.1.2 Covariance evaluations in ENDF/A 19
3.1.3 Uncertainties in Atlas 21
3.2 ^{52}Cr evaluation 26
3.2.1 Capture 28
3.2.2 Elastic scattering 31
3.2.3 Comparison with ENDF/A 36
3.3 ^{56}Fe evaluation 38
3.3.1 Capture 38

3.3.2 Elastic scattering 42
3.4 ^{58}Ni evaluation 46
3.4.1 Capture 46
3.4.2 Elastic scattering 50
3.4.3 Comparison with ENDF/A 51

4 Quality assurance **55**
4.1 Compliance with ENDF-6 format 55
4.2 Mathematical properties of covariance matrices 55
4.3 Cross section uncertainties 56
4.3.1 Integral uncertainties 56
4.3.2 Minimal uncertainties 58
4.4 Dispersion analysis 59
4.4.1 Capture 59
4.4.2 Elastic scattering 61
4.5 Optical model prediction for ^{56}Fe(n,tot) 62

5 Refinements in evaluation procedure **64**
5.1 Modification of default values 64
5.2 Specific changes for ^{52}Cr, ^{56}Fe and ^{58}Ni 65
5.3 Summary of adopted input uncertainties 66

6 Final results **67**
6.1 ^{52}Cr final results 67
6.2 ^{56}Fe final results 71
6.3 ^{58}Ni final results 75
6.4 QA of final results 79

7 Conclusions **81**

Bibliography **83**

Chapter 1

Introduction

In the present work we evaluate covariances for neutron capture and neutron elastic scattering cross sections on several structural materials in the Cr-Fe-Ni mass range using a new covariance formalism developed by us in 2010 [1]. Covariances are needed for a number of applications, such as the Advanced Fuel Cycle Initiative (AFCI) project which employs covariances for data adjustment purposes. The primary objective of the present work is to produce data for an improved AFCI covariance library which will replace earlier releases (AFCI-1.2, September 2009 [2] and AFCI-1.3, April 2010). It is understood that these covariances must be relevant to central cross section values of the latest US evaluated nuclear data library, ENDF/B-VII.0 [3].

Our new formalism produces MF33 cross section covariances and offers several distinct advantages to resonance parameter covariances in file MF32. First, the new formalism is based on analytical expressions and provides a transparent way to propagate resonance parameter uncertainties from the Atlas of Neutron Resonances [4] into cross section covariances. Second, the formalism treats thermal region separately and avoids controversial adjustment of experimentally determined thermal cross section uncertainties to resonance parameter uncertainties. Third, it allows transparent handling of resonance-resonance correlations, often neglected in other methods, with substantial implications for multigroup cross section uncertainties. Forth, it allows inclusion of potential scattering uncertainties into the uncertainty budget and accounting for anti-correlation with the resonance scattering term. Fifth, it avoids the trouble with processing MF32 files with inconsistencies between processing codes NJOY and PUFF. Sixth, the resulting covariances are provided in MF33 format, avoiding the need to harmonize

MF32 with resonance parameters in MF2, making it suitable for *ex post* evaluation of covariances which is often unavoidable for practical reasons.

Evaluation of capture cross section covariances with the new formalism is fairly straightforward. Production of covariances for elastic scattering is more challenging due to several factors, including the presence of high energy resonances which for Cr-Fe-Ni extend to several hundred keV, approximate treatment of interferences, and the trouble with a contribution from external resonances.

The report first summarizes the formalism and then proceeds with details of the evaluation for ^{52}Cr, ^{56}Fe and ^{58}Ni. This is followed by quality assurance analysis which lead to refined evaluation procedure, subsequently applied to produce final covariances for these three major structural materials.

Chapter 2

Evaluation procedure

Detailed description of our evaluation procedure can be found in Ref. [1]. Its key idea is the use of kernel approximation which allowed us to develop analytical formalism of propagating resonance parameter uncertainties [4] into cross sections uncertainties.

2.1 Radiative capture

Thermal and resonance regions are treated separately, the thermal region being determined by the thermal cross section uncertainty readily available in Atlas. In the resonance region we first establish suitable energy bins and determine average cross sections, then compute their uncertainties. To this end we will mostly employ capture kernels readily supplied by Atlas and avoid more involved procedure based on explicit use of resonance parameters. Then, covariance matrix will be constructed using the uncertainties in energy bins, complemented with estimates of correlation coefficients between the energy bins.

2.1.1 Thermal region

In the thermal region capture cross sections in general follow the well-known 1/v law as can be inferred from Westcott factors. As shown in Table 2.1 all structural materials of our interest have Westcott factors close to unity, meaning that they follow 1/v law extremely well.

Table 2.1: Westcott factors g_w for selected materials in ENDF/B-VII.0 library. The values refer to T = 293K and were supplied by S.F. Mughabghab for the purposes of the present report.

Material	g_w	Material	g_w
^{23}Na	0.979	^{54}Fe	0.991
^{50}Cr	0.990	^{56}Fe	0.991
^{52}Cr	0.991	^{57}Fe	0.992
^{53}Cr	0.991	^{58}Ni	0.992
^{55}Mn	0.991	^{60}Ni	0.992

The upper energy limit for applicability of this law is usually considered to be E_{max} = 10 eV, but for structural materials it may extend up to few hundred eV. In practice it might be even higher, depending on the position of the first resonance (typically 1 keV for materials under discussion). In the thermal energy range

$$\sigma_\gamma(E) \approx \sigma_\gamma(E_{th}) \sqrt{\frac{E_{th}}{E}}, \tag{2.1}$$

where E_{th} = 0.0253 eV is the thermal energy. There is only one variable, $\sigma_\gamma(E_{th})$, which determines capture cross sections in the entire thermal energy range. Consequently, uncertainties can be estimated as [1]

$$\Delta\sigma_\gamma(E) \approx \Delta\sigma_\gamma(E_{th}). \tag{2.2}$$

2.1.2 Average cross sections in the resonance region

According to ENDF-6 format radiative capture is well described by the single-level Breit-Wigner (SLBW) formalism. For a single resonance of the energy E_0 the capture cross section at the neutron incident energy E is given as

$$\sigma_\gamma(E) = \pi\lambda\!\!\!^{-2} \frac{g\Gamma_n\Gamma_\gamma}{(E-E_0)^2 + \frac{1}{4}\Gamma^2}, \tag{2.3}$$

[1] This estimate was refined after QA analysis was completed. Adopted refinement leads to considerably improved agreement with resonance integral capture uncertainties. For details see Chapter 5, page 64.

where $\lambda\!\!\!^{-}$ is the de Broglie wavelength (k is the wave number) of the incoming neutron,

$$\lambda\!\!\!^{-} = \frac{1}{k} = \frac{\hbar}{\sqrt{2mE}} \frac{A+1}{A}, \tag{2.4}$$

m being the neutron reduced mass, $\hbar$ the Planck constant and A is the atomic number of target nucleus. The spin statistical factor g is given by

$$g = \frac{2J+1}{2(2I+2)}, \tag{2.5}$$

J being the spin of the resonance and I the spin of the target nucleus. The total resonance width is the sum of partial widths,

$$\Gamma = \Gamma_n + \Gamma_\gamma, \tag{2.6}$$

Γ_n and Γ_γ being the neutron and radiative width, respectively. The capture kernel characterizes the strength of the resonance,

$$A_\gamma = \int_{-\infty}^{+\infty} \sigma_\gamma(E) dE, \tag{2.7}$$

which can be analytically expressed as

$$A_\gamma = 2\pi^2 \lambda\!\!\!^{-2} g \frac{\Gamma_n \Gamma_\gamma}{\Gamma}. \tag{2.8}$$

Considering an isolated resonance of the energy E_0 located in sufficiently broad bin with the energy width

$$\Delta E = E_1 - E_2 \tag{2.9}$$

one gets the average cross section in this energy bin using the capture kernel

$$\bar{\sigma}_\gamma = \frac{1}{\Delta E} \int_{E_2}^{E_1} \sigma_\gamma(E) dE \approx \frac{1}{\Delta E} A_\gamma = a \frac{g \Gamma_n \Gamma_\gamma}{\Gamma}, \tag{2.10}$$

where

$$a = \frac{2\pi^2 \lambda\!\!\!^{-2}}{\Delta E} = 4.089 \times 10^6 \frac{(A+1)^2}{A^2} \frac{1}{E_0 \Delta E} \tag{2.11}$$

is given in units of barn/eV. It should be noted that, up to some fluctuations, the average capture cross section is decreasing rapidly with the incident neutron energy due to $1/E_0$ dependence.

If several resonances are located in a chosen energy interval ΔE, then the average capture cross section is given as

$$\bar{\sigma}_\gamma = \frac{1}{\Delta E} \int_{E_2}^{E_1} \sum_r \sigma_{\gamma r}(E) dE \approx \frac{1}{\Delta E} \sum_r A_{\gamma r} \,, \tag{2.12}$$

where summation goes over all resonances r in this energy bin.

2.1.3 Uncertainties in the resonance region

In order to get uncertainties of average capture cross sections one often employs two different strategies. One can either use available information about capture kernels (usually limited to lower energies) or compute these kernels as explained above. Using a combination of the two might be the best approach, *i.e.*, adopt available kernels whenever available and compute kernels from resonance parameters for remaining energies.

For structural materials the capture kernels as well as their uncertainties are readily provided by the Atlas of Neutron Resonances. In particular, Atlas gives

$$\frac{g\Gamma_n\Gamma_\gamma}{\Gamma} = \frac{1}{a} A_\gamma \tag{2.13}$$

and absolute uncertainty

$$\delta\frac{g\Gamma_n\Gamma_\gamma}{\Gamma} = \frac{1}{a} \delta A_\gamma \,. \tag{2.14}$$

The relative uncertainty of the average capture cross section for a single resonance can be obtained as

$$\Delta\bar{\sigma}_\gamma = \frac{\delta\bar{\sigma}_\gamma}{\sigma_\gamma} = \frac{\delta A_\gamma}{A_\gamma} = \Delta A_\gamma \,. \tag{2.15}$$

We note that kernel uncertainty implicitly takes care about correlation between neutron and radiative widths.

If several resonances are combined together into one energy bin one computes uncertainty from the binomial expression for quadratic summation of uncertainties,

$$(\Delta\bar{\sigma}_\gamma)^2 = \langle \Delta\bar{\sigma}_\gamma \, \Delta\bar{\sigma}_\gamma \rangle = \left\langle \sum_i \Delta A_{\gamma i} \times \sum_r \Delta A_{\gamma r} \right\rangle \,. \tag{2.16}$$

This yields

$$(\Delta\bar{\sigma}_\gamma)^2 = \sum_i \left(\Delta A_{\gamma i}\right)^2 + 2\sum_{i,r} \Delta A_{\gamma i} \left\langle \Delta A_{\gamma i}\, \Delta A_{\gamma r} \right\rangle \Delta A_{\gamma r}\,, \tag{2.17}$$

where $\left\langle \Delta A_{\gamma i}\, \Delta A_{\gamma r} \right\rangle$ is the resonance-resonance (level-level) correlation term. In accordance with Ref.[1] our default values for these correlations for each energy bin are uniformly set up to

$$\mathrm{corr}(A_{\gamma i}, A_{\gamma r}) = \left\langle \Delta A_{\gamma i} \Delta A_{\gamma r} \right\rangle = 0.5. \tag{2.18}$$

2.1.4 Covariance matrix

Covariance matrix is composed of the thermal and resonance components. The covariance in the thermal region is fully self-correlated and hence it reduces to a single diagonal term. In the resonance region the diagonal terms of the covariance matrix are given by the uncertainties of average capture cross sections in chosen energy bins, while the off-diagonal terms represent bin-bin correlation coefficients.

As no information about correlations is available in Atlas, correlation coefficients must be estimated following certain basic principles. In accordance with Eq. (2.18) our default values were set to 0.5.

2.2 Elastic scattering

Similarly to capture, elastic scattering in the thermal and resonance regions will be treated separately. We note, however, that the formalism in the resonance region is much more involved.

2.2.1 Thermal region

Elastic scattering cross sections are nearly constant over a large portion of thermal energy range. At sub-thermal energies, under the free-gas approximation, this constant behavior changes approximately to 1/v due to molecular motion of target nuclei. Thus, at energies defined approximately as $10^{-3}\ eV < E < 10\ eV$, for structural materials extendable up to few hundreds eV, one has

$$\sigma_n(E) \approx \sigma_n(E_{th}). \tag{2.19}$$

At energies below about 10^{-3} eV this relation should be replaced by approximately 1/v behavior which holds for temperatures > 300 K.

Similar to radiative capture there is only variable, $\sigma_n(E_{th})$, which determines cross sections over the entire thermal energy range. Therefore, relative scattering cross section uncertainty in the thermal region can be approximated as[2]

$$\Delta\sigma_n(E) \approx \Delta\sigma_n(E_{th}) = \Delta\sigma_s, \tag{2.20}$$

where σ_s is the free thermal scattering cross section.

2.2.2 Average cross sections in the resonance region

Following ENDF-6 Formats Manual [5] elastic scattering cross section in SLBW representation can be expressed as

$$\sigma_n(E) = 4\pi\lambda\!\!\!^{-2}(2l+1)\sin^2\phi_l + \pi\lambda\!\!\!^{-2} g \frac{\Gamma_n^2 - 2\Gamma_n\Gamma\sin^2\phi_l + 2(E-E_0)\Gamma_n\sin(2\phi_l)}{(E-E_0)^2 + \frac{1}{4}\Gamma^2}, \tag{2.21}$$

where ϕ_l is the phase shift,

$$\phi_0 = kR', \tag{2.22}$$

[2]This estimate should be refined and more conservative estimate applied to neutron energies E >0.5 eV. See Chapter 5, page 64 for more details.

$$\phi_1 = kR' - \arctan(kR') \tag{2.23}$$

and R' is the scattering radius.

Eq. (2.21) has several terms. The first term describes potential scattering, which is nearly constant as a function of energy. The second and third term stand for the symmetric resonance cross section. The last term, containing $2(E - E_0)\Gamma_n \sin(2\phi_l)$ in the numerator, describes interference between potential and resonance scattering which is negative at $E < E_0$ and positive at $E > E_0$. These negative and positive contributions are approximately equal and they cancel out if one computes the average elastic scattering cross section by integrating the cross section over a broad energy interval around the resonance energy E_0.

The average scattering cross section in sufficiently broad energy group of the width $\Delta E = E_1 - E_2$ around the resonance energy E_0 can be obtained as

$$\bar{\sigma}_n = \frac{1}{E_2 - E_1} \int_{E_1}^{E_2} \sigma_n(E) dE = \bar{\sigma}_n^{pot} + \bar{\sigma}_n^{res}. \tag{2.24}$$

The average potential scattering cross section, $\bar{\sigma}_n^{pot}$ and the average resonance elastic scattering cross section, $\bar{\sigma}_n^{res}$, can be approximately expressed analytically.

The resolved resonance region for Cr, Fe and Ni extends up to hundreds of keV, therefore, convenient low-energy approximation is not applicable and one must resort to more complicated expressions. First,

$$\bar{\sigma}_n^{pot} = \frac{1}{E_2 - E_1} \int_{E_1}^{E_2} \sigma_n^{pot}(E) dE \approx 4\pi\lambda\!\!\!^{-2}(2l+1)\sin^2\phi_l\,, \tag{2.25}$$

where the phase shift can be computed at E_0 since $\sigma_n^{pot}(E)$ is slowly varying function of energy. Second,

$$\bar{\sigma}_n^{res} = \frac{1}{E_2 - E_1} \int_{E_1}^{E_2} \sigma_n^{res}(E) dE \approx \frac{\pi\lambda\!\!\!^{-2} g}{E_2 - E_1} \int_{-\infty}^{+\infty} \frac{\Gamma_n^2 - 2\Gamma_n\Gamma\sin^2\phi_l}{(E - E_0)^2 + \frac{1}{4}\Gamma^2} dE, \tag{2.26}$$

where the integral can be computed analytically with the help of the kernel expression

$$A_n = \pi\lambda\!\!\!^{-2} g \int_{-\infty}^{+\infty} \frac{\Gamma_n^2}{(E - E_0)^2 + \frac{1}{4}\Gamma^2} dE = 2\pi^2\lambda\!\!\!^{-2} \frac{g\Gamma_n\Gamma_n}{\Gamma}. \tag{2.27}$$

Considering that $\sin^2\phi_l$ is slowly varying function of energy, one finally gets

$$\bar{\sigma}_n^{res} \approx a\frac{g\Gamma_n(\Gamma_n - 2\Gamma\sin^2\phi_l)}{\Gamma}, \tag{2.28}$$

where a is given by Eq. (2.11) on page 6 and $\sin^2\phi_l$ is computed at E_0.

Eqs. (2.24) and (2.28) have important consequence. While $\bar{\sigma}_n^{pot}$ is approximately constant, the resonance term has $1/E_0$ dependence, hence $\bar{\sigma}_n^{res}$ vanishes with the energy. Therefore, when the resonance region extends to high energies as is the case for structural materials, then neutron elastic scattering becomes determined by potential scattering. As a consequence, elastic scattering uncertainties would be driven by $\Delta R'$ rather than resonance parameter uncertainties.

We note that extension of SLBW to many levels is straightforward by simple summation of SLBW expressions for many resonances. This would represent approximation to more sophisticated multi-level Breit Wigner representation, which takes into account level-level interferences. By using many-level Breit Wigner we assume that negative and positive components of level-level interference terms approximately compensate each other.

2.2.3 External resonances

In general, external resonances with energies below and above the resolved resonance range are added to ENDF-6 formatted files. Bound resonances allow to reproduce thermal cross sections of elastic scattering and capture. High-energy resonances add missing cross section to elastic scattering. These resonances may have extremely large values of Γ_n giving rise to long tails in the elastic scattering cross sections. Thus, for example the bound resonance for ^{52}Cr in ENDF/B-VII.0 is at E_0 = - 870 keV with Γ_n = 710 keV. Such significant external resonances should not be neglected when computing average elastic cross sections with the formalism outlined above.

Since it would be difficult to find suitable analytical expressions for related averages, one can solve the issue numerically. This is facilitated by the fact that no uncertainties are assigned to parameters of external resonances. Therefore, external resonances do not contribute to uncertainties and hence no sensitivities of resonance parameters need to be computed. Using Eq. (2.21) contribution of

external resonance to elastic scattering cross section is

$$\sigma_n^{ex}(E) = \pi \lambda\!\!\!^{-2} g \frac{(\Gamma_n)^2 - 2\Gamma_n \Gamma \sin^2 \phi_l + 2(E - E_0^{ex})\Gamma_n \sin(2\phi_l)}{(E - E_0^{ex})^2 + \frac{1}{4}(\Gamma)^2}, \tag{2.29}$$

where the superscript ex stands for external and the neutron incident energy E is restricted to the resolved resonance range. Thus, for ^{52}Cr this means $1.5\ keV \lessapprox E \lessapprox 1045\ keV$.

We note that one should take into account energy dependence of neutron width when applying Eq. 2.29. Thus, for s-waves

$$\Gamma_n(E) = \Gamma_n \sqrt{\frac{E}{E_0^{ex}}}, \tag{2.30}$$

where Γ_n is the neutron width at E_0^{ex}. This dependence should be taken into account particularly for excessively large neutron widths at energies far away from the resonance energy.

We note that the interference term in Eq. (2.29) is positive for bound levels,

$$E - E_0^{ex} > 0 \quad \text{for} \quad E_0^{ex} \equiv E_0^{bound} < 0 \tag{2.31}$$

and negative for high energy external resonances,

$$E - E_0^{ex} < 0 \quad \text{for} \quad E_0^{ex} \equiv E_0^{high} > E_0^{max}, \tag{2.32}$$

where E_0^{max} is the maximum resonance energy in the resolved resonance region.

As an example, contribution to ^{52}Cr(n,el) cross sections from two bound resonances are shown in Fig. 2.1. Often, different evaluators would chose different parameterization of these resonances, hence we show a case from Atlas and another one from ENDF/B-VII.0.

Contribution to ^{52}Cr(n,el) cross sections from the high-energy resonance is shown in Fig. 2.2 using ENDF/B-VII.0 parametrization, E_0^{high} = -1.2 MeV and Γ_n = 196 keV. One can see that this external resonance would decrease elastic cross sections in not negligible way almost in the entire resonance region. We note that the cross section dip occurs at 1.17 MeV which is very close to the resonance energy E_0^{high} = 1.20 MeV.

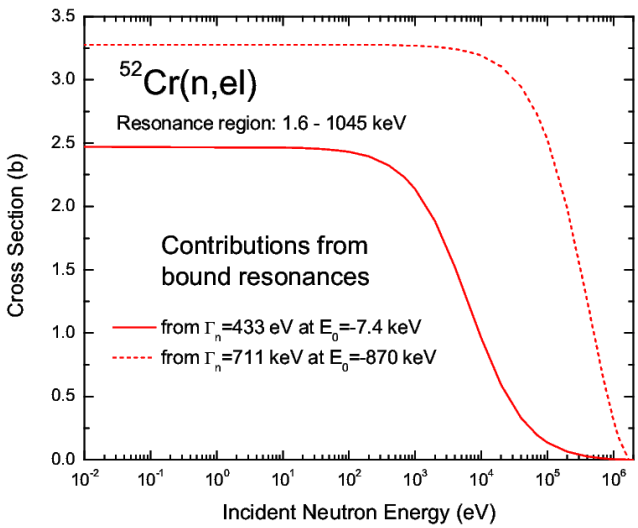

Figure 2.1: Contribution of bound resonances to ^{52}Cr(n,el) cross sections. Results are shown for the resonance at E_0^{bound}= -7.4 keV taken from Atlas, and another one at E_0^{bound}= -870 keV taken from ENDF/B-VII.0 .

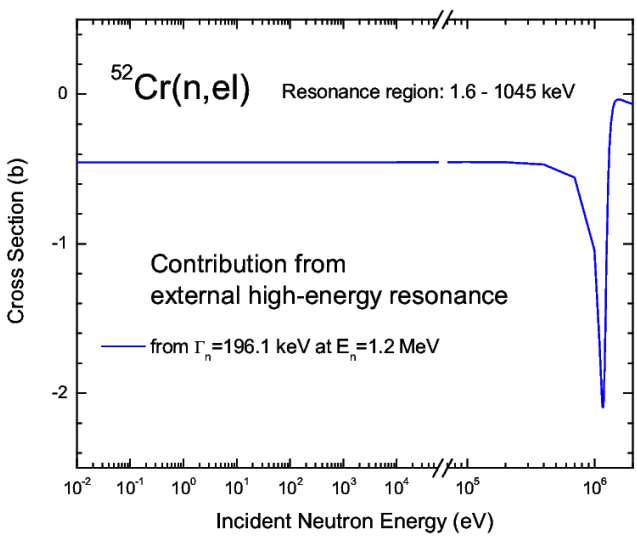

Figure 2.2: Negative contribution of external high-energy resonance to ^{52}Cr(n,el) cross sections. Resonance parameters are those of ENDF/B-VII.0.

2.2.4 Uncertainty for a single resonance

The uncertainty of the average elastic scattering cross section is obtained as quadratic summation of the resonance scattering and potential scattering,

$$(\Delta\bar{\sigma}_n)^2 = \left(\frac{\bar{\sigma}_n^{res}}{\bar{\sigma}_n}\Delta\bar{\sigma}_n^{res}\right)^2 + 2\frac{\bar{\sigma}_n^{res}}{\bar{\sigma}_n}\left\langle\Delta\bar{\sigma}_n^{res}\Delta\bar{\sigma}_n^{pot}\right\rangle\frac{\bar{\sigma}_n^{pot}}{\bar{\sigma}_n} + \left(\frac{\bar{\sigma}_n^{pot}}{\bar{\sigma}_n}\Delta\bar{\sigma}_n^{pot}\right)^2, \tag{2.33}$$

which includes also the correlation term between potential and resonance scattering. What remains to be derived are expressions for relative uncertainties $\Delta\bar{\sigma}_n^{res}$ and $\Delta\bar{\sigma}_n^{pot}$.

Resonance contribution

Sensitivities of the average elastic resonance scattering cross section $\bar{\sigma}_n^{res}$ with respect to Γ_n, Γ_γ and R' can be obtained from Eq. (2.28). One gets

$$\frac{\partial\bar{\sigma}_n^{res}}{\partial\Gamma_n} = ag\frac{\Gamma_n}{\Gamma}\frac{\Gamma+\Gamma_\gamma}{\Gamma} - 2ag\sin^2\phi_l\,, \tag{2.34}$$

$$\frac{\partial\bar{\sigma}_n^{res}}{\partial\Gamma_\gamma} = -ag\frac{\Gamma_n^2}{\Gamma^2} \tag{2.35}$$

and

$$\frac{\partial\bar{\sigma}_n^{res}}{\partial R'} = 4akg\Gamma_n\sin\phi_l\cos\phi_l. \tag{2.36}$$

Using the above expressions for sensitivities the uncertainty for the average resonance scattering cross section can be expressed with the usual quadratic summation as

$$\langle\delta\bar{\sigma}_n^{res}\rangle^2 = \left\langle\frac{\partial\bar{\sigma}_n^{res}}{\partial\Gamma_n}\delta\Gamma_n + \frac{\partial\bar{\sigma}_n^{res}}{\partial\Gamma_n}\delta\Gamma_\gamma + \frac{\partial\bar{\sigma}_n^{res}}{\partial R'}\delta R'\right\rangle^2, \tag{2.37}$$

which yields 3 quadratic terms and 3 cross terms

$$\begin{aligned}\langle\delta\bar{\sigma}_n^{res}\rangle^2 = &\left(\frac{\partial\bar{\sigma}_n^{res}}{\partial\Gamma_n}\delta\Gamma_n\right)^2 + \left(\frac{\partial\bar{\sigma}_n^{res}}{\partial\Gamma_\gamma}\delta\Gamma_\gamma\right)^2 + \left(\frac{\partial\bar{\sigma}_n^{res}}{\partial R'}\delta R'\right)^2 + 2\frac{\partial\bar{\sigma}_n^{res}}{\partial\Gamma_n}\left\langle\delta\Gamma_n\delta\Gamma_\gamma\right\rangle\frac{\partial\bar{\sigma}_n^{res}}{\partial\Gamma_\gamma}\\ &+ 2\frac{\partial\bar{\sigma}_n^{res}}{\partial\Gamma_n}\langle\delta\Gamma_n\delta R'\rangle\frac{\partial\bar{\sigma}_n^{res}}{\partial R'} + 2\frac{\partial\bar{\sigma}_n^{res}}{\partial\Gamma_\gamma}\left\langle\delta\Gamma_\gamma\delta R'\right\rangle\frac{\partial\bar{\sigma}_n^{res}}{\partial R'}.\end{aligned} \tag{2.38}$$

Approximation suitable for Cr, Fe and Ni

All structural materials discussed in the present report are almost pure scatterers, meaning that

$$\Gamma_n >> \Gamma_\gamma \tag{2.39}$$

and hence also absolute uncertainties

$$\delta\Gamma_n >> \delta\Gamma_\gamma. \tag{2.40}$$

As a consequence all terms containing $\delta\Gamma_\gamma$ in Eq. (2.38) can be neglected. On top of it, for materials under discussion there is no correlation between R' and Γ_γ since $\Gamma_n >> \Gamma_\gamma$ and radiative widths could be readily determined from capture cross section measurements. Therefore,

$$\langle\delta\bar{\sigma}_n^{res}\rangle^2 \approx \left(\frac{\partial\bar{\sigma}_n^{res}}{\partial\Gamma_n}\delta\Gamma_n\right)^2 + \left(\frac{\partial\bar{\sigma}_n^{res}}{\partial R'}\delta R'\right)^2 + 2\frac{\partial\bar{\sigma}_n^{res}}{\partial\Gamma_n}\langle\delta\Gamma_n\delta R'\rangle\frac{\partial\bar{\sigma}_n^{res}}{\partial R'} \tag{2.41}$$

and

$$\langle\Delta\bar{\sigma}_n^{res}\rangle^2 \approx \left(\frac{\partial\bar{\sigma}_n^{res}}{\partial\Gamma_n}\frac{\delta\Gamma_n}{\bar{\sigma}_n^{res}}\right)^2 + \left(\frac{\partial\bar{\sigma}_n^{res}}{\partial R'}\frac{\delta R'}{\bar{\sigma}_n^{res}}\right)^2 + 2\frac{\partial\bar{\sigma}_n^{res}}{\partial\Gamma_n}\left\langle\frac{\delta\Gamma_n\delta R'}{\bar{\sigma}_n^{res}\bar{\sigma}_n^{res}}\right\rangle\frac{\partial\bar{\sigma}_n^{res}}{\partial R'}. \tag{2.42}$$

Under the above conditions one has

$$\frac{\partial\bar{\sigma}_n^{res}}{\partial\Gamma_n} \approx \bar{\sigma}_n^{res}\frac{1}{\Gamma_n}$$

and therefore the 1st term of Eq. (2.42) gives

$$\frac{\partial\bar{\sigma}_n^{res}}{\partial\Gamma_n}\frac{\delta\Gamma_n}{\bar{\sigma}_n^{res}} \approx \frac{\delta\Gamma_n}{\Gamma_n} = \Delta\Gamma_n. \tag{2.43}$$

This means that at low energies (low k) and/or small values of $\delta R'$ the relative uncertainties are determined by $\Delta\Gamma_n$ as already shown earlier [1]. The 2nd term of Eq. (2.42) gives

$$\frac{\partial\bar{\sigma}_n^{res}}{\partial R'}\frac{\delta R'}{\bar{\sigma}_n^{res}} \approx \frac{4\sin\phi_l\cos\phi_l}{1-2\sin^2\phi_l}k\delta R', \tag{2.44}$$

which is gaining importance with increasing energy (increasing k). The 3rd term can be easily derived from the first two and it is clear that the anti-correlation between Γ_n and R' should be properly taken into account. On the other hand, at high energies where the 2nd and 3rd term play a role the average elastic scattering cross section $\bar{\sigma}_n$ is determined by potential scattering term and the resonance contribution can be neglected entirely.

Potential scattering contribution

In order to get full contribution from potential scattering one should sum up s-waves and p-waves, while neglecting d-waves and distant level contributions,

$$\sigma_n^{pot}(E) = \frac{4\pi}{k^2}\left\{\sin^2(kR') + 3\sin^2(kR') - \arctan(kR')\right\} \tag{2.45}$$

or

$$\sigma_n^{pot}(E) = \frac{4\pi}{k^2}\left\{\sin^2\phi_0 + 3\sin^2\phi_1\right\}. \tag{2.46}$$

As shown in Ref. [1] one can compute sensitivities analytically and obtain uncertainty of potential scattering cross section as

$$\Delta\bar{\sigma}_n^{pot} = \frac{\partial\bar{\sigma}_n^{pot}}{\partial R'}\frac{\delta R'}{\bar{\sigma}_n^{pot}} = 2\Delta R'\left\{kR'\frac{sin\phi_0\cos\phi_0 + 3\left(1 - \frac{1}{1+(kR')^2}\right)\sin\phi_1\cos\phi_1}{\sin^2\phi_0 + 3\cos^2\phi_1}\right\}, \tag{2.47}$$

where $\Delta R' = \delta R'/R'$ stands for the R' relative uncertainty. The term in complex brackets is the correction factor to the dominant term $2\Delta R'$. This correction factor starts with the value close to 1 and decreases slowly with energy. As an example, for ^{56}Fe it reaches 0.9 at 800 keV [1].

2.2.5 Uncertainty for many resonances

The average cross section due to several resonances located in one energy group can be obtained as

$$\bar{\sigma} = \frac{1}{\Delta E}\int_{E_2}^{E_1}\sum_r \sigma_r(E)dE = \sum_r \bar{\sigma}_r\,, \tag{2.48}$$

where the summation goes over all resonances r in the energy interval ΔE. It should be noted that this equation represents good approximation of capture (and fission), but it is less suitable for elastic scattering, for which multilevel Breit-Wigner or Reich-Moore formalism should be adopted. This means that coherent summation of scattering amplitudes should be applied rather than their incoherent summation assumed by Eq. (2.48). Despite this, the proposed approach should represent sufficiently plausible approximation of elastic cross sections averaged over broad energy groups.

The sensitivities can be computed as partial derivatives of $\bar{\sigma}$ with respect to resonance parameters $p_{i,r}$ where $i = \gamma, n$. Thus,

$$\frac{\partial \bar{\sigma}}{\partial p_{i,r}} = \sum_{r'} \frac{\partial \bar{\sigma}_{r'}}{\partial p_{i,r}} = \frac{\partial \bar{\sigma}_r}{\partial p_{i,r}}, \tag{2.49}$$

meaning that the sensitivity for only one resonance remains on the right hand side, since each resonance is defined by its own set of resonance parameters and does not depend on the parameters of other resonances.

Using these sensitivities the covariance of the group cross section $\bar{\sigma}$ can be obtained as

$$\langle \delta\bar{\sigma}\, \delta\bar{\sigma} \rangle = \sum_{i,r,i',r'} \frac{\partial \bar{\sigma}}{\partial p_{i,r}} \langle \delta p_{i,r}\, \delta p_{i',r'} \rangle \frac{\partial \bar{\sigma}}{\partial p_{i',r'}}, \tag{2.50}$$

where $\langle \delta p_{i,r}\, \delta p_{i',r'} \rangle$ is the covariance of resonance parameters.

By dividing Eq. (2.50) with the average cross section one gets expression for the relative covariance

$$\frac{\langle \delta\bar{\sigma}\, \delta\bar{\sigma} \rangle}{\bar{\sigma}^2} = \sum_{i,r,i',r'} \frac{1}{\bar{\sigma}} \frac{\partial \bar{\sigma}_r}{\partial p_{i,r}} \langle \delta p_{i,r}\, \delta p_{i',r'} \rangle \frac{1}{\bar{\sigma}} \frac{\partial \bar{\sigma}_{r'}}{\partial p_{i',r'}}. \tag{2.51}$$

Using explicit expressions for the sensitivities derived in the previous Chapter and making appropriate assumptions about the correlations between the resonance parameter uncertainties one can get the uncertainty of the average cross section in a given energy bin.

2.2.6 Correlation coefficients

Correlation coefficients have values between -1.0 and +1.0. In the above equations they are defined as

$$\langle \Delta p_1 \Delta p_2 \rangle = \frac{\langle \delta p_1 \delta p_2 \rangle}{\delta p_1 \delta p_2}. \tag{2.52}$$

We will also use notation

$$\mathrm{corr}(p_1, p_2) = \langle \Delta p_1 \Delta p_2 \rangle. \tag{2.53}$$

A summary of the default values of the correlation coefficients proposed in Ref. [1] is given in Table 2.2.

Table 2.2: Default values of correlation coefficients (range -1.0 to +1.0).

No.	Type	Quantity	Default
1	Single resonance	corr(Γ_n, Γ_γ)	0.0
2	Resonance-resonance	corr($\Gamma_\gamma, \Gamma_\gamma$)	0.5
3	Resonance-resonance	corr(Γ_n, Γ_n)	0.5
4	Resonance-resonance	corr(Γ_n, Γ_γ)	0.0
5	Pot. scattering-resonance	corr(R', Γ_n)	-0.5
6	Bin-bin	corr($\bar{\sigma}_\gamma, \bar{\sigma}_\gamma$)	0.5
7	Bin-bin	corr($\bar{\sigma}_n, \bar{\sigma}_n$)	0.5
8	Thermal-resonance	corr($\sigma_\gamma^{th}, \bar{\sigma}_\gamma$)	0.0
9	Thermal-resonance	corr($\sigma_n^{th}, \bar{\sigma}_n$)	0.0
10	Cross-correlation	corr($\sigma_n^{th}, \sigma_\gamma^{th}$)	0.0
11	Cross-correlation	corr($\sigma_n^{res}, \sigma_\gamma^{res}$)	0.0

2.2.7 Covariance matrix

The very last step of our procedure is creation of the covariance matrix. This step is fairly straightforward and similar to what was used in the case of radiative capture.

Thus, the covariance matrix is composed of the thermal and resonance components. The covariance in the thermal region is fully self-correlated and hence it reduces to a single diagonal term. In the resonance region the diagonal terms of the covariance matrix are given by the uncertainties of average capture cross sections in chosen energy bins, while the off-diagonal terms represent bin-bin correlation coefficients.

Default values of bin-bin correlation coefficients are given in Table 2.2; actual values should be determined by an evaluator keeping in mind that no information is available in Atlas of Neutron Resonances. Therefore, one must resort to estimates following certain basic principles discussed in Ref. [1].

Chapter 3

Evaluations

3.1 Preparatory analysis

3.1.1 List of materials

In the mass region of most important structural materials, Cr-Fe-Ni, one finds 15 stable nuclides shown in Table 3.1. Among them are 9 materials, ^{50,52,53}Cr, ^{55}Mn, ^{54,56,57}Fe and ^{58,60}Ni, for which AFCI data adjustment project needs covariances with high and medium priority. The highest priority is given to three materials, ^{52}Cr, ^{56}Fe and ^{58}Ni, due to their high natural abundance. We note that evaluation of ^{55}Mn has been already described in Ref. [1].

3.1.2 Covariance evaluations in ENDF/A

Several new evaluations have been completed recently by ORNL in the resonance region. This work was funded by the US Nuclear Criticality Safety Program. The files can be found in ENDF/A library which stores candidate evaluations for the forthcoming release of ENDF/B-VII.1 scheduled for November 2011.

ENDF/A evaluations relevant to the present work are listed in Table 3.2. They include 5 materials, the first author being either Luiz Leal or Herve Derrien. All evaluations have been performed with the code SAMMY. Unfortunately, description of covariance procedures in MF1/MT451 is either virtually non-existent or fairly short.

Table 3.1: Stable nuclides in the Cr-Fe-Ni mass region. Given is natural abundance, ground state spin, maximum energy in the resonance region (Atlas) and AFCI priority.

No.	Z	Nucleus	Abundance %	Spin	E_0^{max} keV	Priority
1	24	^{50}Cr	4.3	0	591	medium
2		^{52}Cr	83.8	0	1045	high
3		^{53}Cr	9.5	3/2	264	medium
4		^{54}Cr	2.4	0	590	low
5	25	^{55}Mn	100.0	5/2	208	medium
6	26	^{54}Fe	5.8	0	807	medium
7		^{56}Fe	91.8	0	850	high
8		^{57}Fe	2.1	1/2	190	medium
9		^{58}Fe	0.3	0	348	low
10	27	^{59}Co	100.0	7/2	119	low
11	28	^{58}Ni	68.1	0	811	high
12		^{60}Ni	26.2	0	451	medium
13		^{61}Ni	1.2	3/2	69	low
14		^{62}Ni	3.6	0	600	low
15		^{64}Ni	0.9	0	583	low

Thus, description by Leal of ^{52}Cr [6] and ^{53}Cr [7] reduces to a single sentence. SAMMY was used and covariances are given in the form of the resonance parameter covariance matrix (RPCM) stored in file MF32. We note that ^{52}Cr contain also covariances in the fast neutron region by Perreslavtsev *et al* [8].

Descriptions by Derrien are more detailed and provide some useful hints. Evaluation of ^{55}Mn [9] currently contains only MF32 data. We note that the evaluators recognize deficiencies in this file and systematic experimental uncertainties being added as MF33 (*D. Wiarda, private communication, Port Jeff, June 2009*). This seems to be already done for ^{58}Ni [10] and ^{60}Ni [11]. For these two latter materials systematic experimental uncertainties were explicitly added as MF33,

Table 3.2: Summary of new covariance evaluations in ENDF/A relevant to the present work. These evaluations were performed with the code SAMMY.

Material	1st author	Ref.	Year	Comment
^{52}Cr	Leal	[6]	2009	MF32, fast region MF33 [8]
^{53}Cr	Leal	[6]	2009	MF32 only
^{55}Mn	Derrien	[9]	2009	MF33 added in 2010
^{58}Ni	Derrien	[10]	2009	MF33 already included
^{58}Ni	Derrien	[11]	2009	MF33 already included

with all non-diagonal correlation coefficients set up arbitrarily to 0.5.

3.1.3 Uncertainties in Atlas

Resonance parameter uncertainties of Cr-Fe-Ni materials play critical role in our procedure. Availability of these data in Atlas of Neutron Resonances is summarized in Table 3.3. For example, for ^{56}Fe resolved resonance region extends up to 850 keV, neutron width uncertainties are available up to 260 keV, capture width uncertainties up to 260 keV and uncertainties of capture kernels also up to 260 keV; uncertainty of the average radiative width for s-waves is 52% and for p-waves 39%.

Scattering radii and their uncertainties, $\Delta R'$, are summarized in Table (3.4). These are important quantities as they essentially determine elastic scattering uncertainties at high resonance energies. Values of $\Delta R'$ are those given in Atlas. For light nuclei they were in general deduced from thermal data.[1] Adopted $\Delta R'$ values are estimated and they are much higher in view of considerable difference between the thermal and resonance energies. As a rule we use the following estimate[2]

$$\Delta R'(E_{res}) \approx 2\Delta R'(E_{th}). \tag{3.1}$$

[1]For nuclei with Z > 90 only in few cases R' and $\Delta R'$ were derived from data in the resonance region, values of R' are based also on scattering data in the energy region up to 400 keV.

[2]Factor of two was considered to be too conservative once QA analysis was completed. More refined values were adopted in the final run. For details see Chapter 5, page 64.

Table 3.3: Availability of resonance parameter uncertainties in Atlas for 9 structural materials. For $\Delta\Gamma_n, \Delta\Gamma_\gamma$ and ΔA_γ maximum resonance energies are given. For $\langle\Delta\Gamma_{\gamma 0}\rangle$ and $\langle\Delta\Gamma_{\gamma 1}\rangle$ relative uncertainties are given.

Nucleus	E_0^{max} keV	$\Delta\Gamma_n$ E_0^{max}	$\Delta\Gamma_\gamma$ E_0^{max}	ΔA_γ E_0^{max}	$\langle\Delta\Gamma_{\gamma 0}\rangle$ %	$\langle\Delta\Gamma_{\gamma 1}\rangle$ %	Comments
^{50}Cr	591	472	292	297	50[a)]	31	Gaps in $\Delta\Gamma_n$, $\Delta\Gamma_\gamma$
^{52}Cr	1045	1045	490	490	50[a)]	11	
^{53}Cr	264	244	264	200	50[a)]	33	
^{55}Mn	208	208	112	-	20	25	Gaps in $\Delta\Gamma_\gamma$
^{54}Fe	807	807	195	195	50[a)]	26	
^{56}Fe	850	260	260	260	52	39	
^{57}Fe	190	190	190	190	60	86	Gaps in $\Delta\Gamma_\gamma$, $\Delta\Gamma_n$
^{58}Ni	811	811	447	447	57	43	
^{60}Ni	451	451	445	451	31	6	

[a)] No uncertainty available in Atlas, value of 50% is estimated.

Thermal cross section uncertainties for 9 structural materials are summarized in Table (3.5).

When dealing with elastic scattering one should also be aware of external resonances, in particular bound resonances. These are summarized in Table 3.6. One can see that in most cases bound resonance would not cause a problem for kernel approximation. An exception is ^{58}Ni with two bound resonances and neutron width 20 keV and 15 keV. Such large values are explained by the need to recover exceptionally large thermal elastic scattering of 25.3 b, which by far exceeds potential scattering contribution.

Table 3.6 also shows ENDF/B-VII.0 bound levels if considerable differences exist with Atlas. A notable case is ^{52}Cr where ENDF/B-VII.0 has bound level at E_0 = -870 keV with huge neutron width Γ_n = 710 keV.

Table 3.4: Scattering radii and their uncertainties for 9 structural materials. Values of $\Delta R'$ are those given in Atlas, deduced from thermal data as well as low energy resonance region. For example, ^{56}Fe, the interference minimum at 24 keV was considered to pin down R'. Initially adopted $\Delta R'$ values in the resonance region follow Eq. (3.1). Values adopted in final analysis are also shown, see Chapter 5, page 64 for justification.

Nucleus	E_0^{max} keV	VII.0 R' fm	Atlas, at E_{th} R' fm	$\Delta R'$ fm	$\Delta R'$ %	Adopted $\Delta R'(E_{res})$ %	Note
^{50}Cr	591	5.37	5.0	0.3	6.0		
^{52}Cr	1045	5.44	5.4	0.3	5.6	11.2	Final value 8.3%
^{53}Cr	264	5.48	5.4	0.3	5.6		
^{55}Mn	208	5.15	4.5	0.4	8.9	17.8	
^{54}Fe	807	5.48	5.0[a]	-	-		
^{56}Fe	850	5.44	5.9[b]	0.3	5.1	10.2	Final value 5.1%
^{57}Fe	190	5.90	6.1[c]	-	-		
^{58}Ni	811	6.30	6.4[d]	0.2	3.1	6.2	Final value 3.1%
^{60}Ni	451	6.00	6.7	0.3	4.5		

a) ^{54}Fe: R'is not available in Atlas; present value estimated by SFM in July 2010; ENDF/B-VII.0 for p-wave resonances is R'_1 = 3.70 fm

b) ^{56}Fe: ENDF/B-VII.0 for p-wave resonances is R'_1 = 4.90 fm

c) ^{57}Fe: R'is not available in Atlas; present value estimated by SFM in July 2010

d) ^{58}Ni: ENDF/B-VII.0 for p-wave resonances is R'_1 = 4.23 fm

Table 3.5: Thermal cross section uncertainties for 9 structural materials. Shown are uncertainties given in Atlas, in the low-fidelity project and adopted values. Also shown are absolute values of thermal cross sections in ENDF/B-VII.0 and Atlas.

Nucleus	Reaction	VII.0 +)	A t l a s			Lowfi *)	Adopted	Note
	σ	σ	σ	$\Delta\sigma$	$\Delta\sigma$	$\Delta\sigma$	$\Delta\sigma$	
	b	b	b	b	%	%	%	
^{50}Cr	(n,γ)	15.9	15.4	0.2	1.3	1.7	2.0	
	(n,el)	2.37	2.41	0.06	2.5	-	2.5	
^{52}Cr	(n,γ)	0.75	0.86	0.02	2.3	7.1	3.0	1)
	(n,el)	2.99	2.96	0.02	0.67	0.67	2.5	2)
^{53}Cr	(n,γ)	18.1	18.6	0.6	3.2	3.3	3.3	
	(n,el)	7.92	7.76	0.20	2.6	2.6	2.6	
^{55}Mn	(n,γ)	13.4	13.36	0.05	0.37	0.4	0.8	3)
	(n,el)	2.19	2.06	0.03	1.50	2.5	3.0	4)
^{54}Fe	(n,γ)	2.25	2.25	0.18	8.0	8.0	8.0	
	(n,el)	2.20	2.17	0.10	4.6	4.6	4.6	
^{56}Fe	(n,γ)	2.59	2.59	0.14	5.4	5.4	5.4	5)
	(n,el)	12.16	12.62	0.49	3.9	4.0	4.0	6)
^{57}Fe	(n,γ)	2.43	2.48	0.30	12	12	12	
	(n,el)	2.62	0.68	0.06	8.8	58	50	7)
^{58}Ni	(n,γ)	4.62	4.37	0.10	2.3	2.8	4.0	8)
	(n,el)	25.0	25.3	0.40	1.6	1.6	1.6	9)
^{60}Ni	(n,γ)	2.76	2.50	0.06	2.4	5.0	5.0	
	(n,el)	0.98	0.98	0.07	7.1	7.1	7.1	

+) Taken from www.nndc.bnl.gov/sigma at 300K (March 23, 2010).

*) Taken from www.nndc.bnl.gov/lowfi (March 23, 2010).

1) ^{52}Cr(n,γ): 0.75 ± 0.02 (2.7%) in 2009 ORNL eval (ENDF/A), rounded value adopted

2) ^{52}Cr(n,el): 3.07 ± 0.07 (2.3%) in 2009 ORNL eval (ENDF/A), rounded value adopted

3) ^{55}Mn(n,γ): 0.8% adopted in agreement with IRDF-2 assessment (IAEA, 2008)

4) ^{55}Mn(n,el): 3% adopted to account for discrepancy between Atlas and ENDF/B-VII.0

5) ^{56}Fe(n,γ): Atlas value adopted; 6) ^{56}Fe(n,el): Atlas value adopted

7) ^{57}Fe(n,el): Note also huge discrepancy between major data libraries.

8) ^{58}Ni(n,γ): 4% adopted to account for discrepancy between Atlas and ENDF/B-VII.0

9) ^{58}Ni(n,el): Atlas value adopted

Table 3.6: Parameters of bound resonances for selected structural materials taken from Atlas of Neutron Resonances. Some values taken from ENDF/B-VII.0 are shown for comparison.

Nucleus	E_0 keV	J	Γ_n eV	Γ_γ eV	Comment
^{50}Cr	-0.359	1/2	3.18	1.09	
^{52}Cr	-8.700	1/2	7.1e5	2.055	ENDF/B-VII.0
	-7.375	1/2	433	2.0	
	-6.808	1/2	4.2e5	14.46	ENDF/B-VII.0
^{53}Cr	-1.189	2	26.1	2.3	
	-0.320	1	2.59	2.3	
^{55}Mn	-1.615	3	6.26e3	0.75	
	-0.203	2	1.15	0.75	
^{54}Fe	-21.9	1/2	7.73e3	1.6	
^{56}Fe	-6.52	1/2	1.39e3	1.474	
^{57}Fe	-3.61	1	177	1.9	
^{58}Ni	-50	1/2	2.01e4	1.48	
	-28.5	1/2	1.56e4	8	
^{60}Ni	-4.17	1/2	22.5	1.37	

3.2 ^{52}Cr evaluation

Evaluation is performed in several consecutive steps. We start with inspecting capture and elastic scattering cross sections to get a feeling about possible challenges. Then, we identify energy binning for average cross sections, compute uncertainties for these average cross sections and afterwards produce covariance matrices.

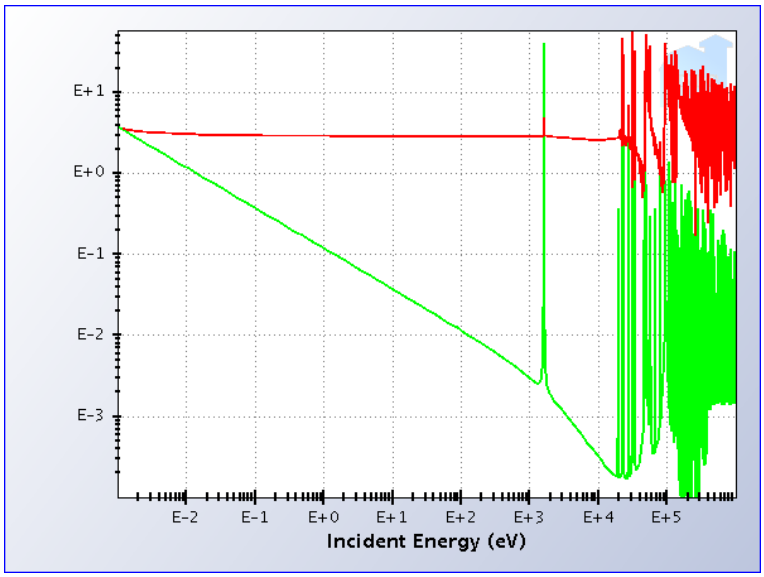

Figure 3.1: ^{52}Cr capture (green) and elastic (red) cross sections in the thermal and resonance region. The 1st resonance is at 1.63 keV (p-wave), followed by strong resonance at 31.6 keV (s-wave). Data were taken from ENDF/B-VII.0; plots were produced by the NNDC retrieval and plotting system Sigma.

^{52}Cr(n,γ) and (n,el) cross sections in ENDF/B-VII.0 library are shown in Fig. 3.1. The plots reveal certain basic features of these cross sections. Thus, capture in the thermal region follows 1/v pretty well up to about 400 eV, while elastic is approximately constant up to about 1.5 keV and with some tolerance even up to about 19 keV. Except for very low energies, capture cross sections are much smaller than elastic cross sections. Elastic cross section exhibits strong interferences.

Fig. 3.2, showing the average cross sections for ENDF/B-VII.0 data, illustrates

in more quantitative way relationship between capture cross sections and elastic cross sections. We used energy binning discussed later in the text. One can see that capture is about 3 orders of magnitude smaller than elastic scattering cross sections. This observation has considerable consequence on certain practical considerations faced by an evaluator. The most important of them is negligible impact of correlation coefficients between radiative and neutron widths on covariances.

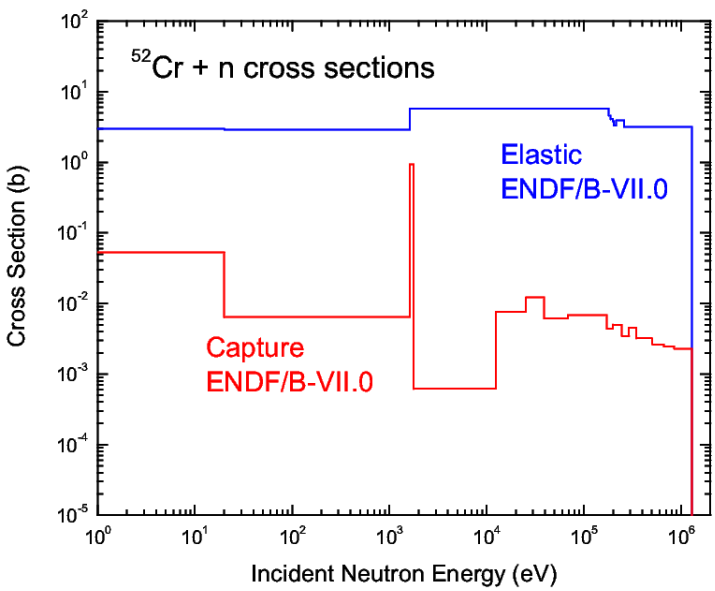

Figure 3.2: ^{52}Cr capture (red) and elastic (blue) from ENDF/B-VII.0. Group structure for NJOY processing is chosen to match energy binning adopted in the present work.

3.2.1 Capture

The first step in the evaluation is decision on energy binning to be adopted for computing average capture cross sections. Our choice is shown in Fig. 3.3 where comparison is made with correct values obtained by processing ENDF-6 formatted file with NJOY. One can see that up to few minor discrepancies the agreement is excellent in the entire energy range.

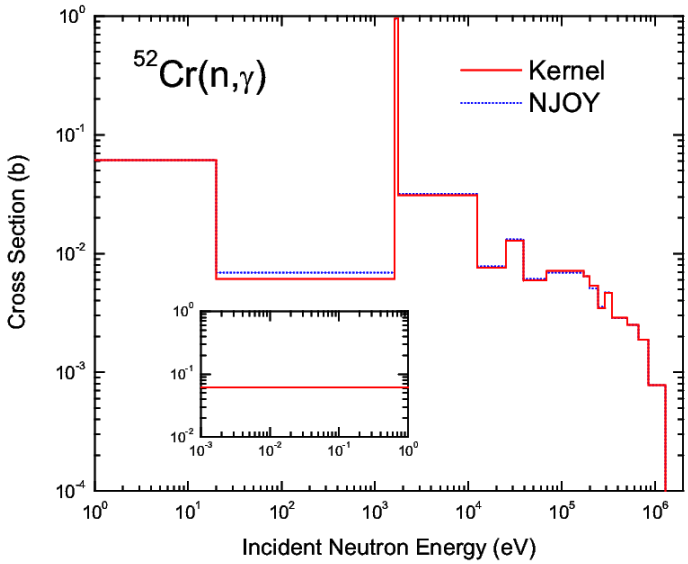

Figure 3.3: Comparison of average cross sections for ^{52}Cr capture obtained from kernels (above 1.5 keV) and from NJOY in the whole energy range. Below 1.5 keV the kernel values are obtained from 1/v dependence normalized to thermal cross section. Shown in the insert is the energy region from 10^{-3} eV to 10 eV. All data are based on Atlas.

The second step is computing uncertainties for these average cross sections. The results are shown in Fig. 3.4, making it clear that impact of correlations between individual resonances is very strong. This is particularly true for the high energy bins. One can see that use of $\mathrm{corr}(\Gamma_\gamma, \Gamma_\gamma) = 0.0$ would lead to unrealistically low and flat uncertainties. In general, high energy bins contain large amount of resonances, therefore, $\sqrt{N}$ reduction of uncertainties becomes very pronounced if correlations are not considered. Even though for ^{52}Cr(n,γ) there is quite a bit of fluctuations of radiative widths in part due to valence direct capture, effective

number of resonances is still high. Thus, for example in the energy bin 350-500 keV, one should account for $N_{eff} \approx 20$ out of N = 30. This explains why corr = 1.0 leads to uncertainty of 36% $\approx \sqrt{20} \times 8\%$ compared to 8% for corr = 0.0.

We adopted default value of corr($\Gamma_\gamma, \Gamma_\gamma$) = 0.5 which is mid-way between 0.0 and 1.0 to address this issue. The resulting high energy uncertainty of 30% is in line with fairly small average capture cross sections of about 1-2 mb in this energy range.

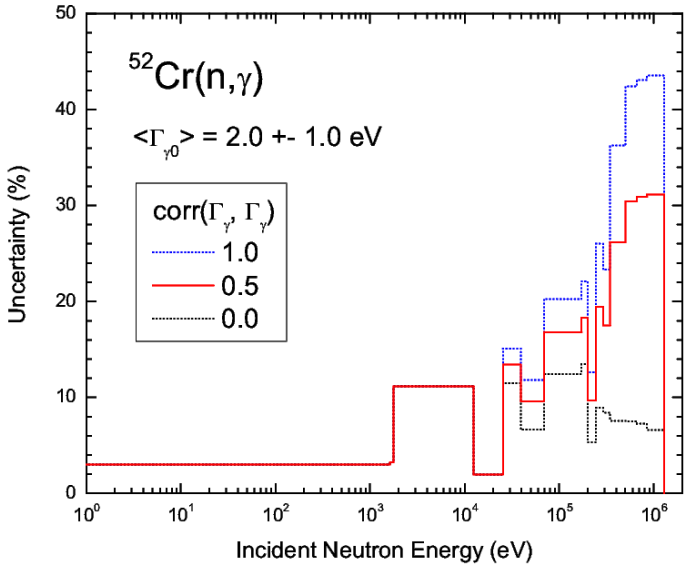

Figure 3.4: Relative uncertainties of average cross sections for ^{52}Cr capture. Shown are results for three values of resonance-resonance correlation coefficients, corr($\Gamma_\gamma, \Gamma_\gamma$), applied uniformly within each energy bin. Impact of corr(Γ_n, Γ_n) on capture is marginal.

The third and final step is construction of covariance matrix for capture. The result depends on adopted values of bin-bin correlations. Fig. 3.5 shows three options that we explored. In accordance with our choice for corr($\Gamma_\gamma, \Gamma_\gamma$) = 0.5 discussed above, our preference for bin-bin correlation is also 0.5, with results shown to the right top.

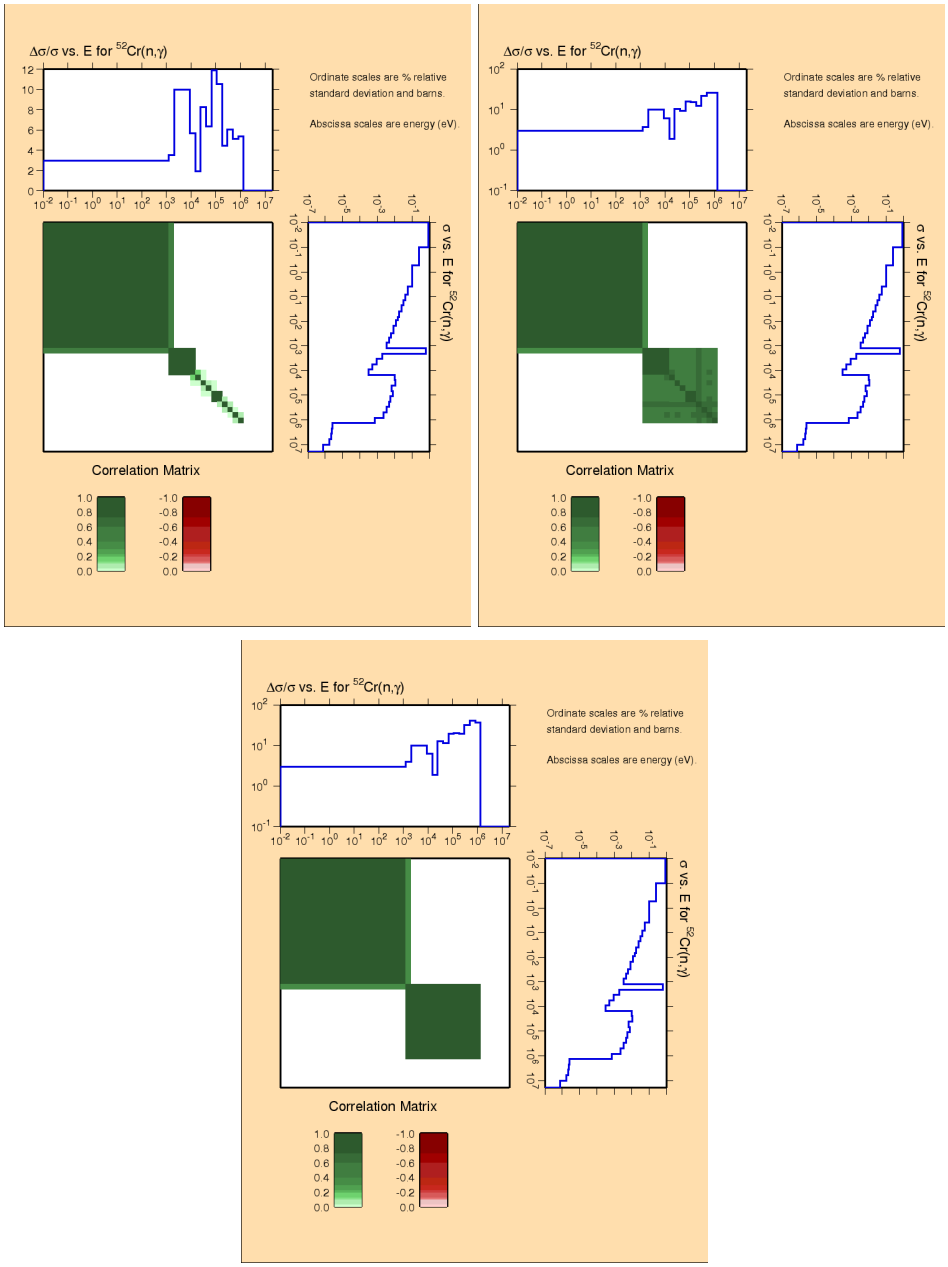

Figure 3.5: Covariances for ^{52}Cr capture in 33-energy groups for three values of resonance-resonance and bin-bin correlation coefficients: 0.0 (top left), 0.5 (adopted, top right) and 1.0 (bottom).

3.2.2 Elastic scattering

Similar to evaluation of capture covariances we proceed in three steps. First, we determine energy binning and compute average scattering cross sections. Second, we produce uncertainties for these average cross sections. Third, we combine these uncertainties into full covariance matrices.

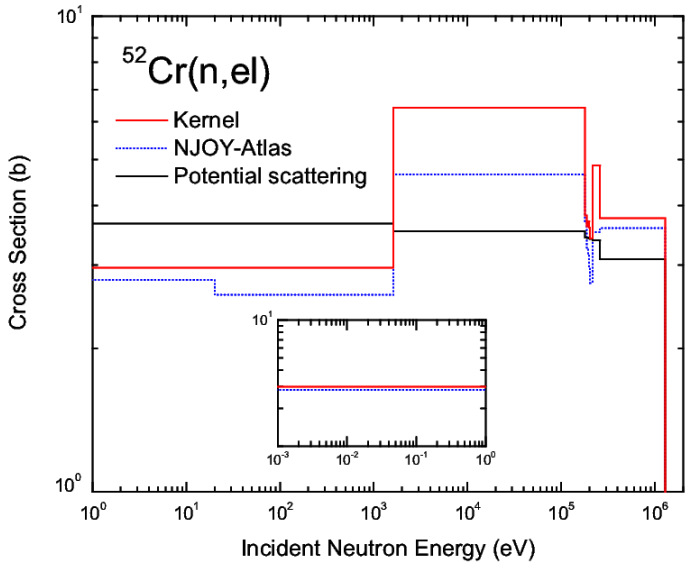

Figure 3.6: Comparison of average cross sections for ^{52}Cr elastic scattering obtained from kernels (above 1.5 keV) and from NJOY in the whole energy range. The kernel values in the thermal region (below 1.5 keV) were obtained directly from the thermal cross section. Shown in the insert is the energy region from 10^{-3} eV to 10 eV. All data are based on Atlas.

^{52}Cr(n,el) represents one of the most difficult cases for kernel approach. This can be seen in Fig. 3.6 which shows average elastic cross sections. The thermal region extends up to about 1.5 keV. Even though we adopted very broad bin structure in the resonance region, with much reduced number of bins compared to capture, the agreement with NJOY is relatively modest. This explains why the first bin in the resonance energy range is so broad (1.5 keV - 200 keV). There is fairly good agreement in the highest energy bin (300 keV - 1050 keV).

Another important observation refers to the average potential scattering cross sections. One can see that the role of potential scattering about above 200 keV is very strong compared to the resonance term. Consequently, $\Delta R'$ would play dominant role in determining related elastic scattering uncertainties.

In view of these difficulties additional analysis was done. Kernel values based on Atlas were compared with correct average cross section obtained by NJOY using ENDF/B-VII.0 (see Fig. 3.7). One can see that agreement is reasonable and in support of using kernel approximation for the purposes of uncertainty estimate.

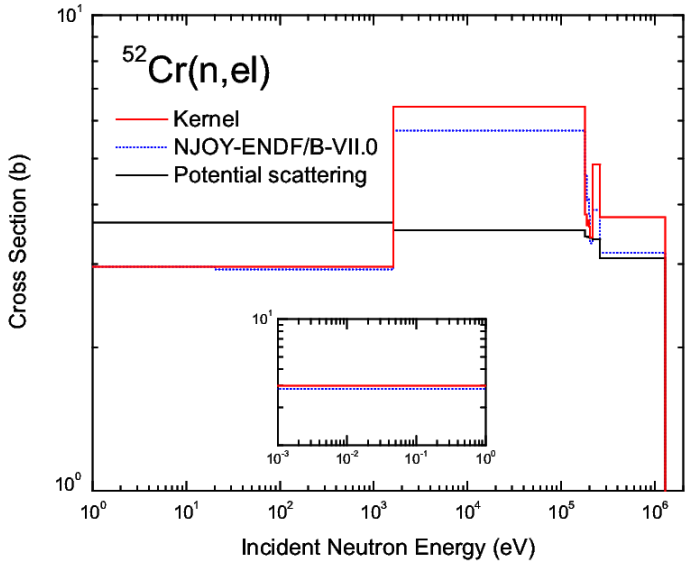

Figure 3.7: Average cross sections for ^{52}Cr(n,el). Compared are kernel values based on Atlas parametrization with NJOY based on ENDF/B-VII.0 parametrization.

As the second step, uncertainties for adopted energy bins were computed. Results shown in Fig. 3.8 include potential scattering contribution assuming $\Delta R' = 11.1\%$. Uncertainties in the resonance region are in the range of about 10-15%, with some tendency for growth with the energy.

Fig. 3.8 reveals that the role of correlations between neutron widths is small. This can be explained by two factors. First, each bin has single dominant neutron resonance which essentially determines uncertainty, the remaining resonances in

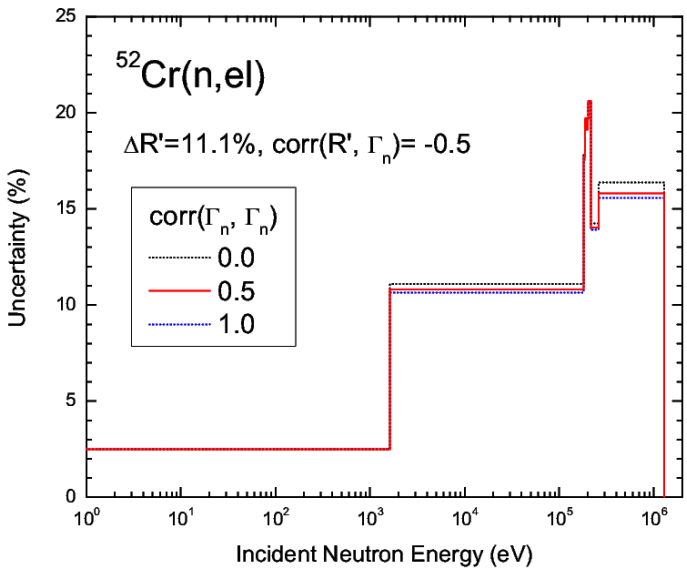

Figure 3.8: Uncertainties of ^{52}Cr(n,el)average cross sections. Shown are results for three values of resonance-resonance correlation coefficients, corr(Γ_n, Γ_n), adopted uniformly for each energy bin. Impact of corr($\Gamma_\gamma, \Gamma_\gamma$) on scattering is marginal.

that bin being relatively weak. Second, role of potential scattering is strong, diminishing any contribution from the resonance scattering term. As expected, due to $\Gamma_n >> \Gamma_\gamma$ impact of correlations between radiative widths is completely negligible.

Fig. 3.9 clarifies the role of potential scattering in cross section uncertainties. This is shown by comparing full uncertainties with the case of hypothetical $\Delta R'$ = 0. One can clearly see that the role of potential scattering is indeed very strong. Ignoring this term would lead to flat uncertainty curve with some tendency to decline from 2.5% in the thermal region to approximately 2% at about 1 MeV, which is deemed to be unrealistic.

Full covariances matrices were constructed from bin uncertainties under specific assumptions about bin-bin correlations. Shown in Fig. 3.10 are results for 3 scenarios of bin-bin correlations, 0.0, +0.5 and +1.0. The differences are relatively weak, we adopted our default value +0.5.

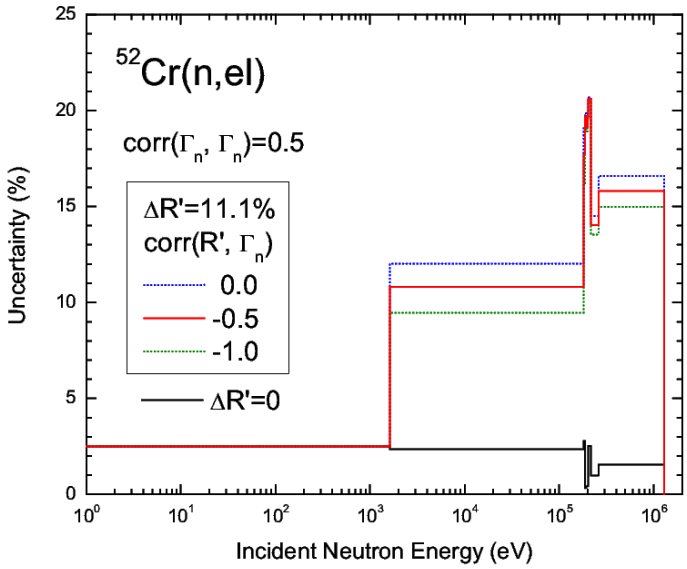

Figure 3.9: Uncertainties of average cross sections for ^{52}Cr(n,el) for two values of $\Delta R'$. Used in both cases were default values of correlation coefficients, corr(Γ_n, Γ_n) = 0.5 and corr(R', Γ_n) = -0.5.

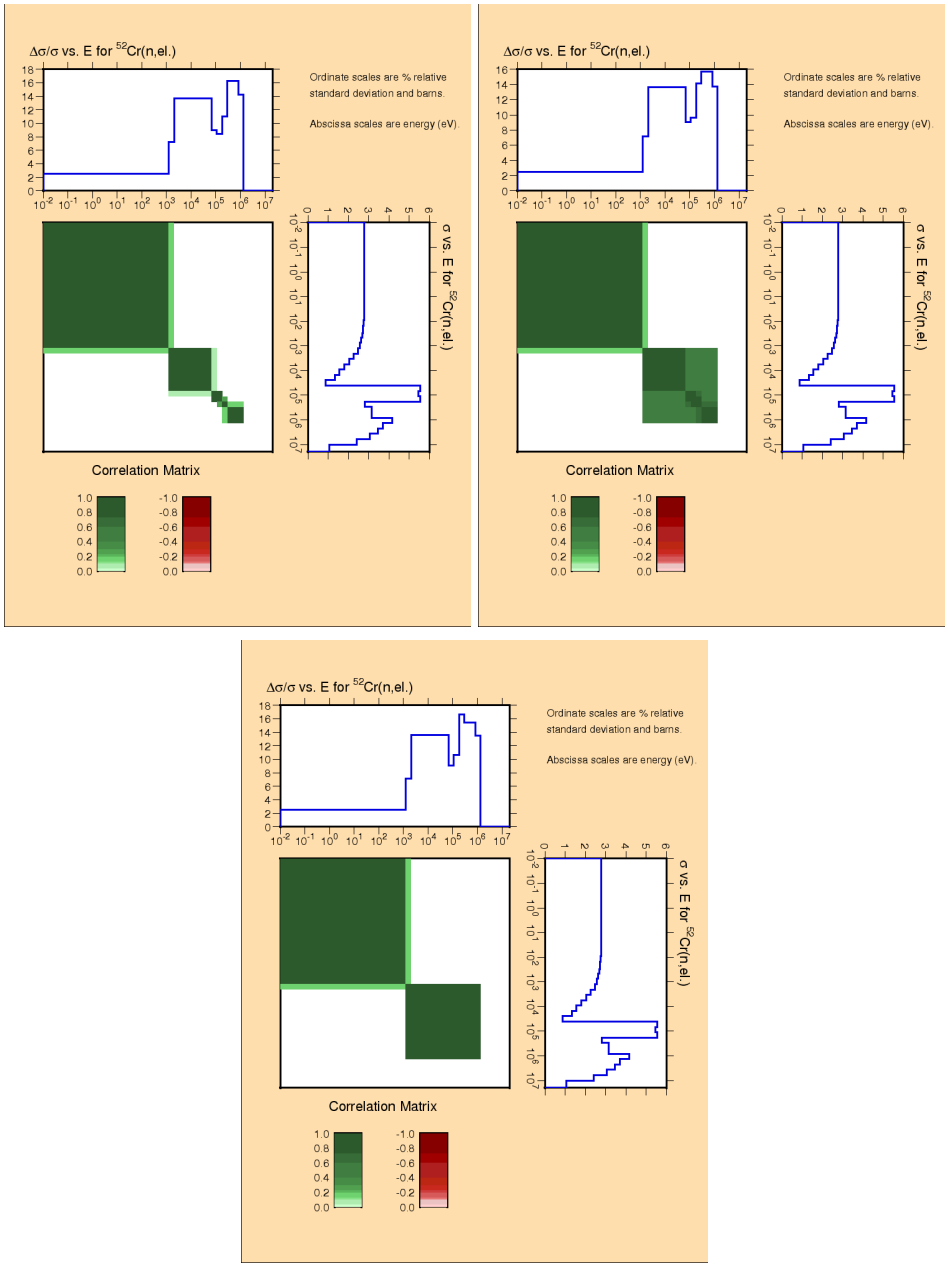

Figure 3.10: Covariances for ^{52}Cr elastic scattering in 33-energy groups for three values of resonance-resonance and bin-bin correlation coefficients: 0.0 (top left), 0.5 (adopted, top right) and 1.0 (bottom).

3.2.3 Comparison with ENDF/A

It is instructive to compare our covariances with those produced by Leal *et al*, ORNL in 2009 [6]. Fast region was supplied by Pereslavtsev *et al*, Karlsruhe [8]. This file can be found in ENDF/A library which collects candidate evaluations for the forthcoming ENDF/B-VII.1 release. Covariances in the resonance region were produced with the code SAMMY; data are stored in MF32 file.

Comparison of essential features of the results obtained in the present work and ENDF/A is given in Table 3.7. Shown are uncertainties in the thermal region and at the high end of the resonance region. Differences are striking both for capture and elastic scattering. In both instances thermal uncertainties are grossly overestimated in ENDF/A. At the high energy end of the resolved resonance region (about 1 MeV) the uncertainties are again completely opposite; this time ENDF/A claiming much better precision compared to our results.

Table 3.7: Relative uncertainties of ^{52}Cr+n cross sections obtained in the present work compared with ENDF/A [6]. Also shown are values from JENDL-4.0 library released in May 2010 [12]. Uncertainties were obtained from full covariance files by processing into 33-group energy structure.

Reaction	Energy	Uncertainty			Comment
		Present	ENDF/A	JENDL-4.0	
^{52}Cr(n,γ)	Thermal	3%	20%	2%	Error in ENDF/A
	1 MeV	30%	3%	2%	Lack of corr in ENDF/A?
^{52}Cr(n,el)	Thermal	2.5%	6.5%	1%	Error in ENDFA
	1 MeV	15%	2%	0.3%	No $\Delta R'$ in ENDF/A

For ^{52}Cr(n,γ) the reasons for these differences can be at least partly explained. The thermal region in ENDF/A seems to be in obvious error, caused by MF33 data supplied by Karlsruhe for the fast neutron and extended by error down to the thermal region *(L. Leal, private communication, April 2010)*. In the high energy end of the resonance region the capture uncertainty in ENDF/A is unrealistic since one can argue that 2% precision for 1-2 mb cross section is very optimistic. Observed decline in ENDF/A uncertainties suggests that long-range correlations

were not taken into account.

In the case of ^{52}Cr(n,el), ENDF/A uncertainty in the thermal region is far too high and most likely in error. At about 1 MeV ENDF/A is much lower than our results most likely as the consequence of failing to account for contribution from the potential scattering. On the other hand, at least to some extent, our results can be also challenged as they directly depend on our estimate of $\Delta R'$. However, even if we would adopt the lower value, $\Delta R' = 5.6\%$, rather than 11.1% our uncertainties would be still much larger than ENDF/A.

Brand new JENDL-4.0 library released in May 2010 [12] contains ^{52}Cr covariances in the resonance region. These were taken over from the ORNL evaluation with the caveat that JENDL-4.0 eliminated MF33 file by Karlsruhe and kept only MF32 file. This explains the difference between ENDF/A and JENDL-4.0 in Table 3.7. The uncertainty at about 1 MeV of 0.3% is very low. It is comparable with the best determined standard cross section of 0.2% for H(n,el) and much better than 0.5% precision reached for another standard, C(n,el). Thus, 0.3% uncertainty for ^{52}Cr(n,el) can hardly be viewed as realistic.

3.3 ^{56}Fe evaluation

In performing this covariance evaluation we proceeded similarly to ^{52}Cr. The logic of the procedure is very much the same, hence we restrict ourselves to showing our results graphically.

Capture cross sections as well as elastic scattering cross sections retrieved by Sigma from ENDF/B-VII.0 are shown in Fig. 3.11. The 1/v behavior in thermal region for capture extends up to 200 eV and with some tolerance even up to 1 keV Elastic scattering cross sections remain fairly constant, starting from the thermal energy up to about 300 eV. Processed cross sections can be seen in Fig. 3.12.

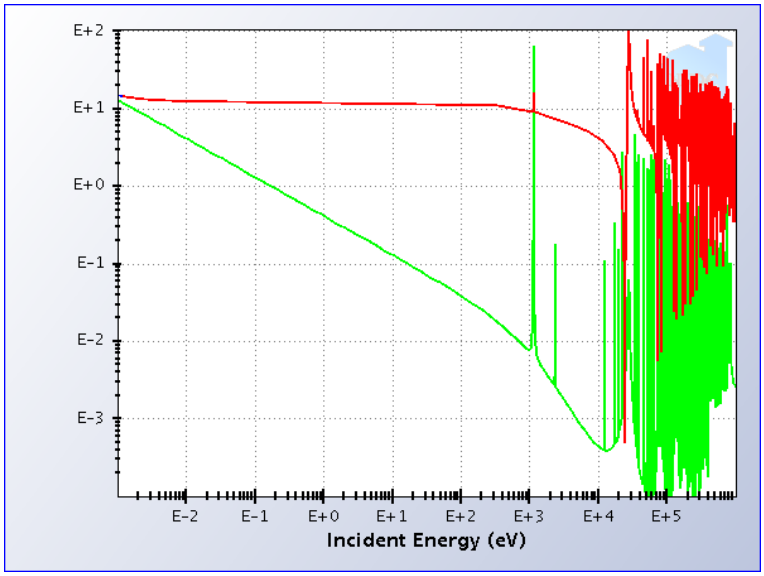

Figure 3.11: ^{56}Fe capture (green) and elastic (red) cross sections in the thermal and resonance region. The 1st resonance is at 1.15 keV (p-wave), followed by strong resonance at 27.8 keV (s-wave). Data were taken from ENDF/B-VII.0; plots were produced by the NNDC retrieval and plotting system Sigma.

3.3.1 Capture

Evaluation of capture covariances is done in three steps: energy binning for average cross sections, uncertainties of these averages, combining bins into full co-

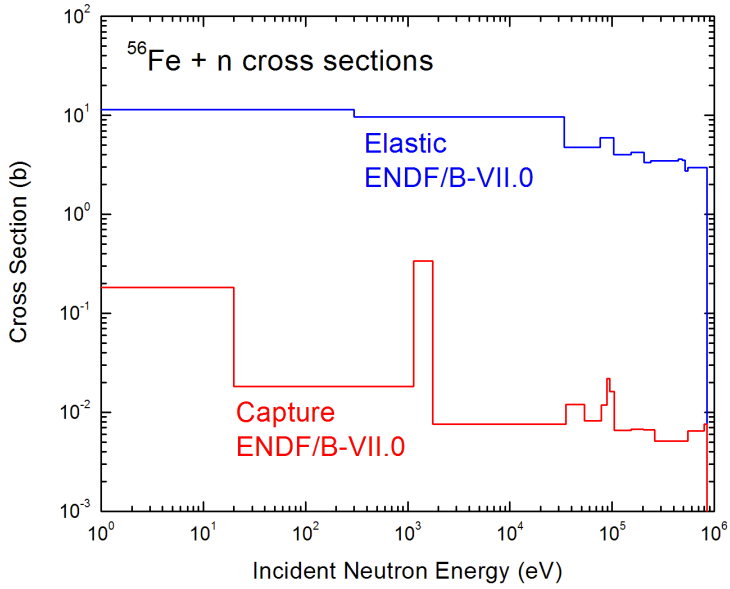

Figure 3.12: ^{56}Fe capture (red) and elastic (blue) from ENDF/B-VII.0. Group structure for NJOY processing is chosen to match energy binning adopted in the present work.

variance matrix.

Average capture cross sections can be seen in Fig. 3.13 showing very good agreement with the correct results obtained by NJOY. We note that Atlas contains almost 290 resonances which were combined into 14 energy bins. We start with a single resonance in the lowest resonance bin, followed by 5 resonances in the 2nd bin, *etc.* up to about 80 resonances in the highest bin.

Uncertainties of average cross sections can be seen in Fig. 3.14. We show three scenarios of resonance-resonance correlations and their strong impact on the final result. For corr($\Gamma_\gamma, \Gamma_\gamma$) = 0.0 the uncertainties tend to decrease and are ultimately somewhat lower than 5% for the thermal cross section. This is not plausible given strong decline of about 3 orders of magnitude of capture cross section in this energy range. Our choice is corr($\Gamma_\gamma, \Gamma_\gamma$) = 0.5.

Full covariance matrix is shown in Fig. 3.15. Adopted were default values of bin-bin correlation coefficients, 0.5, across the board.

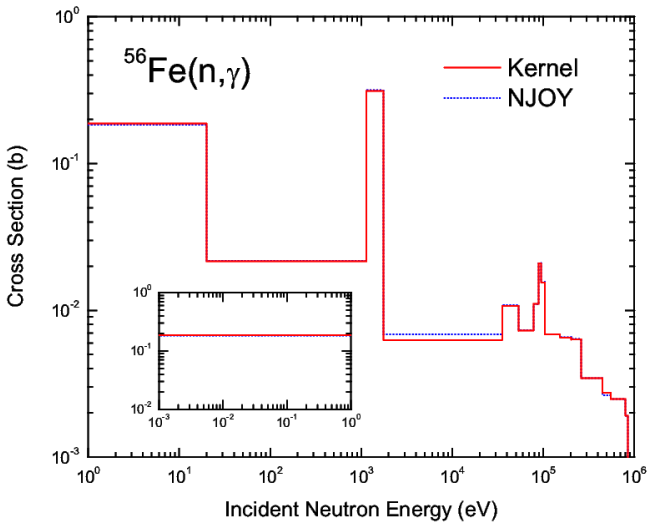

Figure 3.13: Average cross sections for ^{56}Fe(n,γ) from kernels (above 1 keV) compared with NJOY (whole energy range). Insert shows energies from 10^{-3} eV to 10 eV.

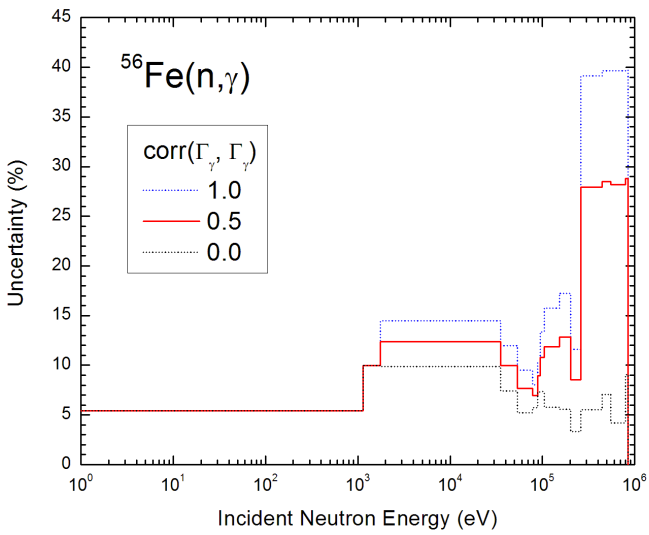

Figure 3.14: Relative uncertainties of average cross sections for ^{56}Fe capture. Shown are results for different values of resonance-resonance correlation coefficients, corr$(\Gamma_\gamma, \Gamma_\gamma)$, applied uniformly within each energy bin. Impact of corr(Γ_n, Γ_n) on capture is marginal.

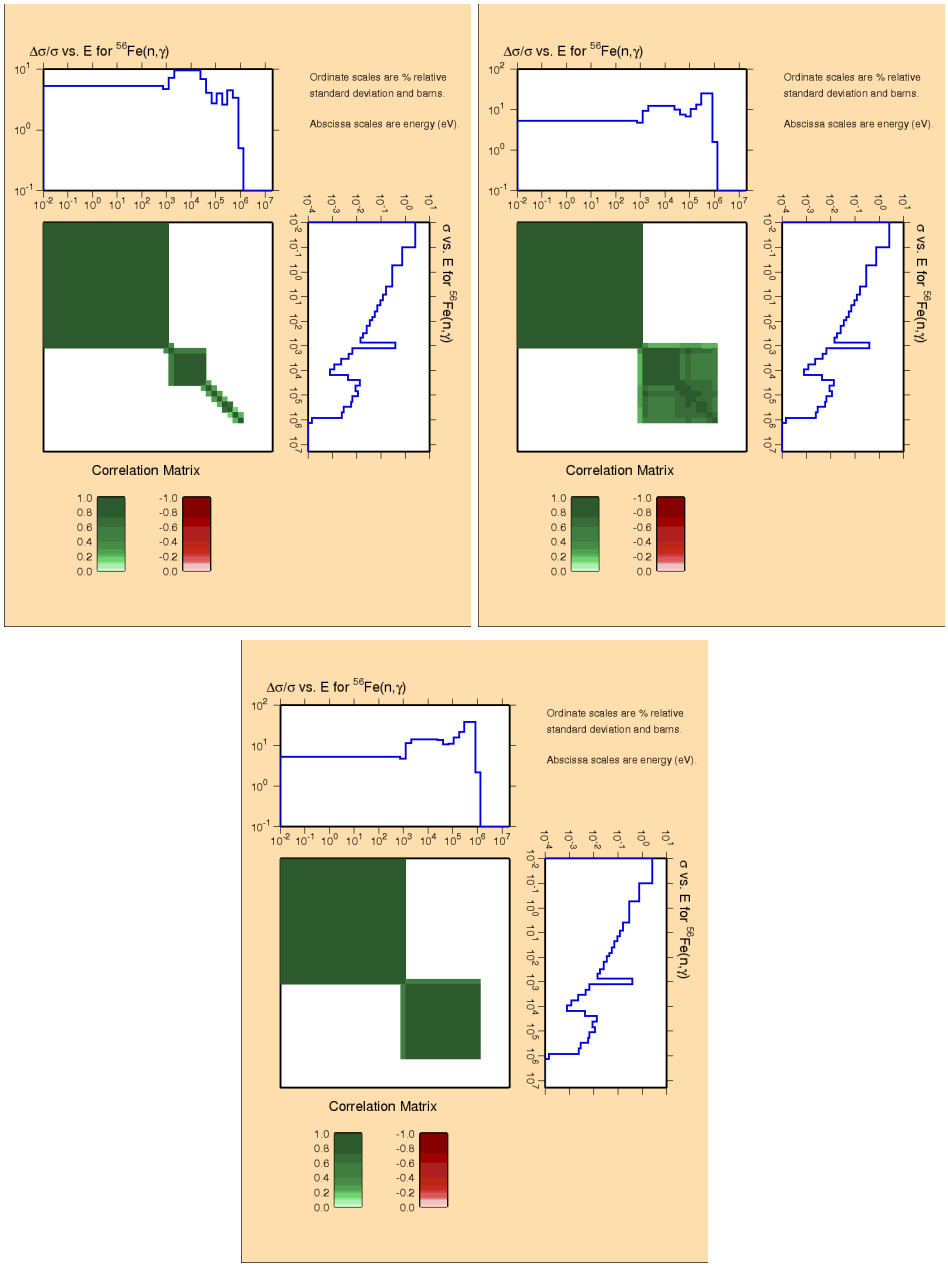

Figure 3.15: Covariances for ^{56}Fe capture in 33-energy groups for three values of resonance-resonance and bin-bin correlation coefficients: 0.0 (top left), 0.5 (adopted, top right) and 1.0 (bottom).

3.3.2 Elastic scattering

Evaluation is again performed in three steps, similar to how we proceeded in the case of ^{52}Cr(n,el).

First, we determine energy binning and calculate average elastic scattering cross sections in these bins. These results are shown Fig. 3.16. One can see that fairly good agreement with NJOY was achieved, except for the region around 100 keV. One can also see that potential scattering is strong in the resonance region above about 30 keV and becomes dominant at the high energy end of this region. Thus, in the highest energy bin $\bar{\sigma}_{pot} \approx 3.7$ b and $\bar{\sigma}_{res} \approx 1$ b. Consequently, when the uncertainties for elastic scattering are produced by weighted quadratic summation of the potential and resonance contributions, then the weight of the potential scattering term would be about 10 times larger than that of the resonance term.

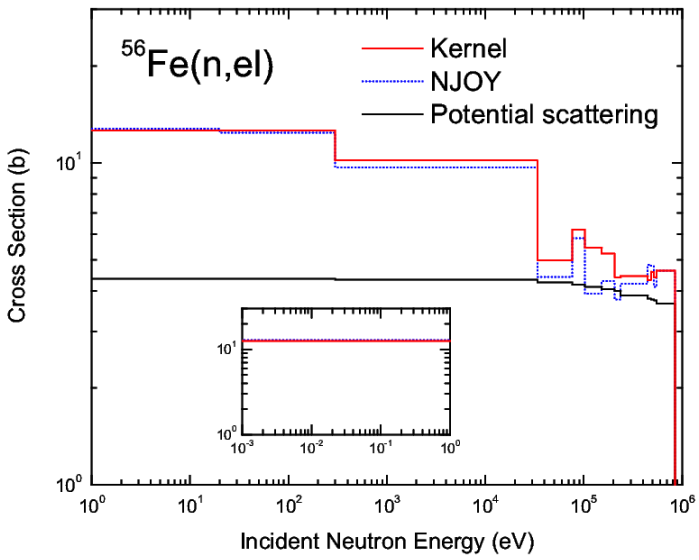

Figure 3.16: Comparison of average cross sections for ^{56}Fe elastic scattering obtained from kernel (above 300 eV) and from NJOY in the whole energy range. The kernel values in the thermal region (below 300 eV) were obtained directly from the thermal cross section. Shown in the insert is the energy region from 10^{-3} eV to 10 eV.

Second, we compute uncertainties as shown in Fig. 3.17. One can see that from 4% at the thermal region the uncertainties keep growing, with some flucta-

tions, and reach about 15% at the high energy end of the resonances region. This is in line with our estimate of $\Delta R' = 10.2\%$ which implies that potential scattering uncertainty is $2\Delta R' \approx 20\%$.

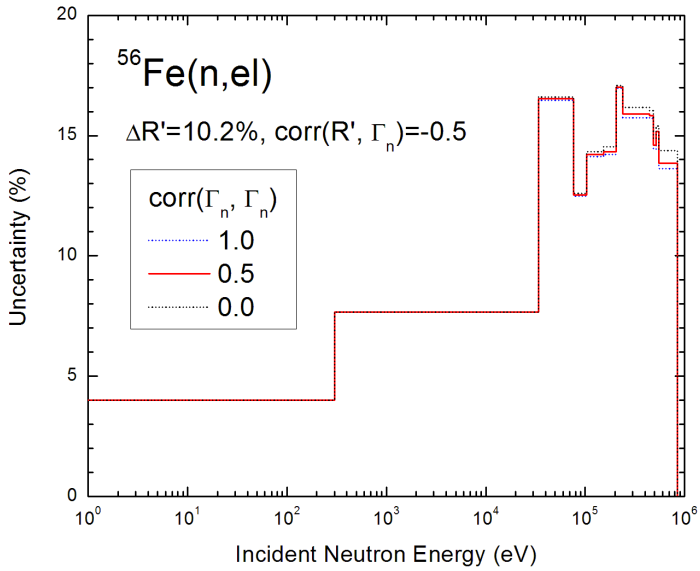

Figure 3.17: Uncertainties of ^{56}Fe(n,el) average cross sections. Shown are results for three values of resonance-resonance correlation coefficients, corr(Γ_n, Γ_n), adopted uniformly for each energy bin. Impact of corr($\Gamma_\gamma, \Gamma_\gamma$) on scattering is marginal.

Fig. 3.18 shows strong impact of potential scattering on the uncertainty. Ignoring potential scattering contribution would lead to nearly flat uncertainties with values close to 1% as can be seen on the curve computed for $\Delta R' = 0$. Such low values are in general considered unrealistic. For example, reactor analysts believe that plausible values are around 8-10% *(G. Palmiotti, INL, private communication, December 2009)*. If so, this would indicate that our estimate of $\Delta R'$ is too conservative, see Chapter 5, page 64 for improved estimate.

Finally, we combine these bin uncertainties into full covariance matrix, Fig. 3.19. Default values were adopted for correlation coefficients.

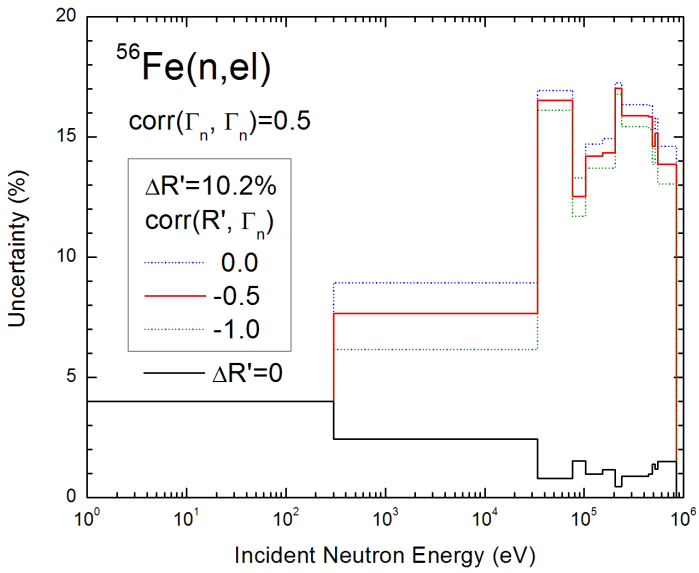

Figure 3.18: Uncertainties of ^{56}Fe(n,el) average cross sections for two values of $\Delta R'$. Used in both cases were default values of correlation coefficients, corr(Γ_n, Γ_n) = 0.5 and corr(R', Γ_n) = -0.5.

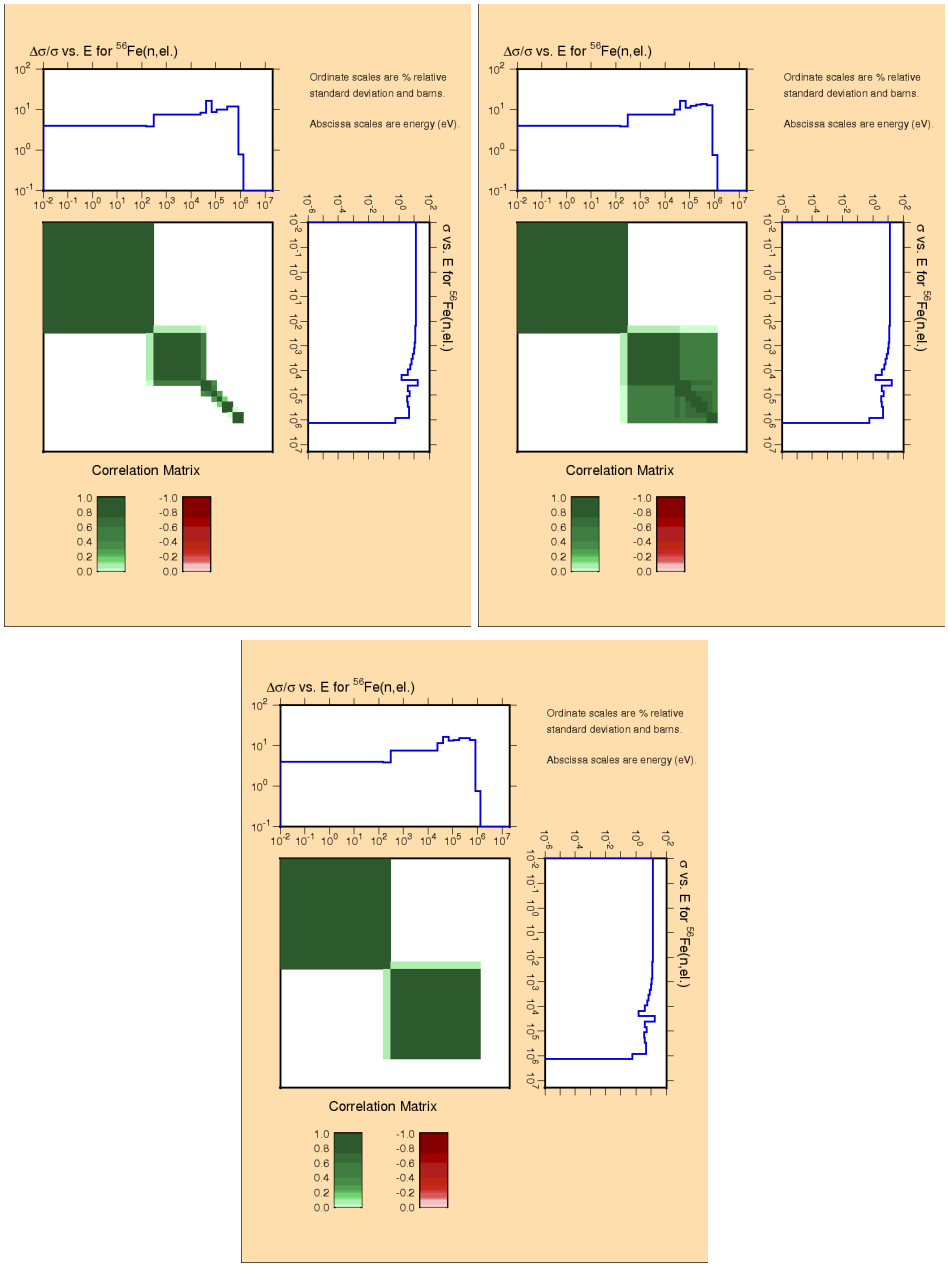

Figure 3.19: Covariances for ^{56}Fe elastic scattering in 33-energy groups for three values of resonance-resonance and bin-bin correlation coefficients: 0.0 (top left), 0.5 (adopted, top right) and 1.0 (bottom).

3.4 ^{58}Ni evaluation

Capture and elastic cross sections in the thermal and resonance region are displayed in Fig. 3.20. For capture cross section the region of 1/v behavior extends up to about 2 keV and with some tolerance perhaps even up to 6 keV. Elastic cross section is fairly constant from about 0.01 eV up to about 1 keV; interference effects are strong.

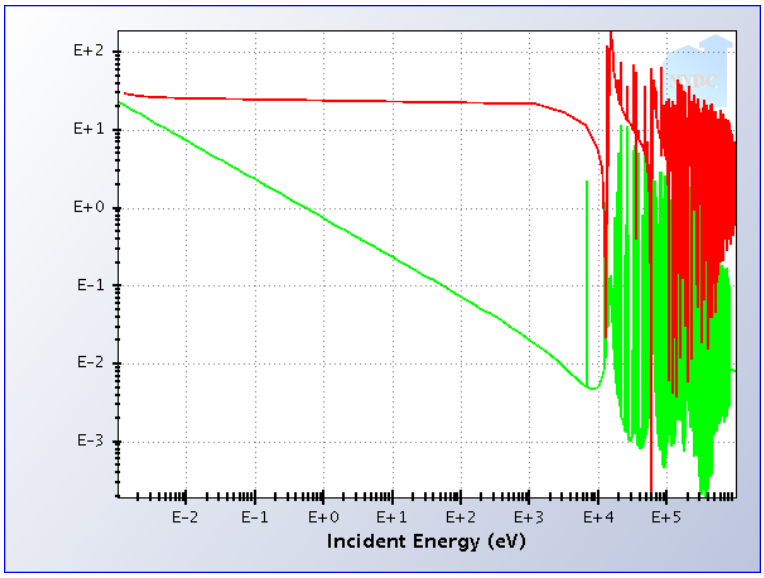

Figure 3.20: ^{58}Ni capture (green) and elastic (red) cross sections in the thermal and resonance region. The 1st resonance is at 6.9 keV (p-wave), followed by strong resonance at 15.3 keV (s-wave). Data were taken from ENDF/B-VII.0; plots were produced by the NNDC retrieval and plotting system Sigma.

Fig. 3.21 shows the same cross sections processed by NJOY into the multigroup structure adopted in the present work. One can see that capture cross section is 2-3 orders of magnitude lower than the elastic scattering.

3.4.1 Capture

Evaluation of ^{58}Ni(n,γ) is again performed in three steps, the same as for ^{52}Cr and ^{56}Fe capture. First, one determines energy binning and calculate average capture

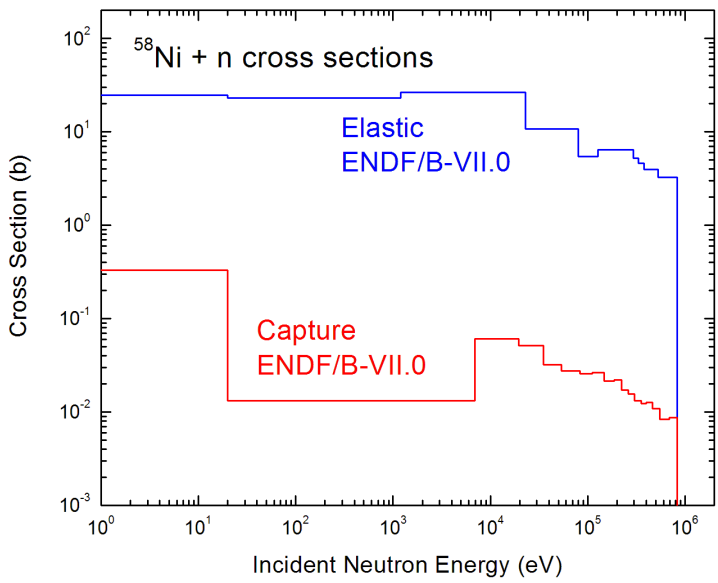

Figure 3.21: ^{58}Ni capture (red) and elastic (blue) from ENDF/B-VII.0. Group structure for NJOY processing is chosen to match energy binning adopted in the present work.

cross sections in these bins. Our results can be seen Fig. 3.22, illustrating excellent agreement of kernel approximation with the precise results obtained by NJOY.

Second, one computes uncertainties, see Fig. 3.23. We note strong impact of adopted correlations between radiative widths of individual resonances in each energy bin. As already noted for ^{52}Cr and ^{56}Fe corr($\Gamma_\gamma, \Gamma_\gamma$) = 0.0 produces unrealistic uncertainties and should be excluded. Therefore, we adopted the value of 0.5.

Finally, one combines these partial uncertainties into full covariance matrix. This is shown in Fig. 3.24. We adopted default values for correlation coefficients, *i.e.*, 0.5 across the board.

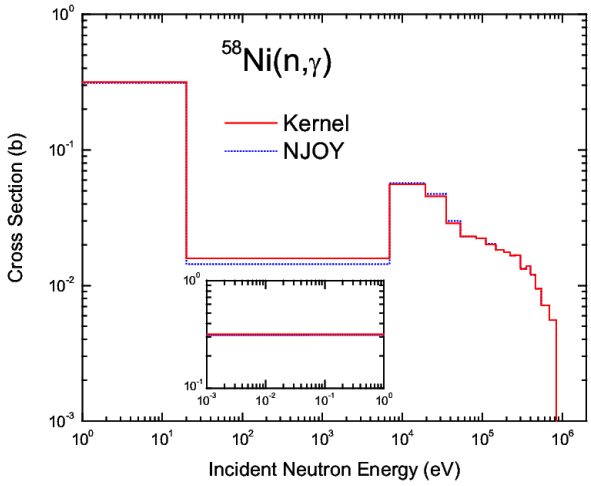

Figure 3.22: ^{58}Ni(n,γ) average cross sections from kernels (above 6 keV) are compared with NJOY (whole energy range). Below 6 keV we used 1/v dependence normalized to thermal cross section. Insert shows energies from 10^{-3} eV to 10 eV.

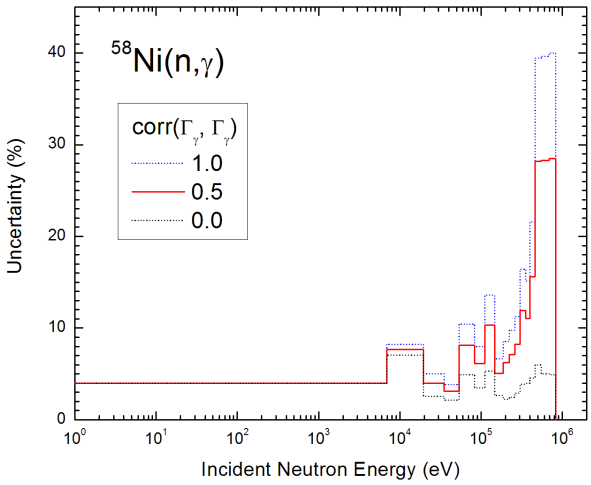

Figure 3.23: Relative uncertainties of ^{58}Ni(n,γ) average cross sections. Shown are results for three values of resonance-resonance correlation coefficients, corr($\Gamma_\gamma, \Gamma_\gamma$), applied uniformly within each energy bin. Impact of corr(Γ_n, Γ_n) on capture is marginal.

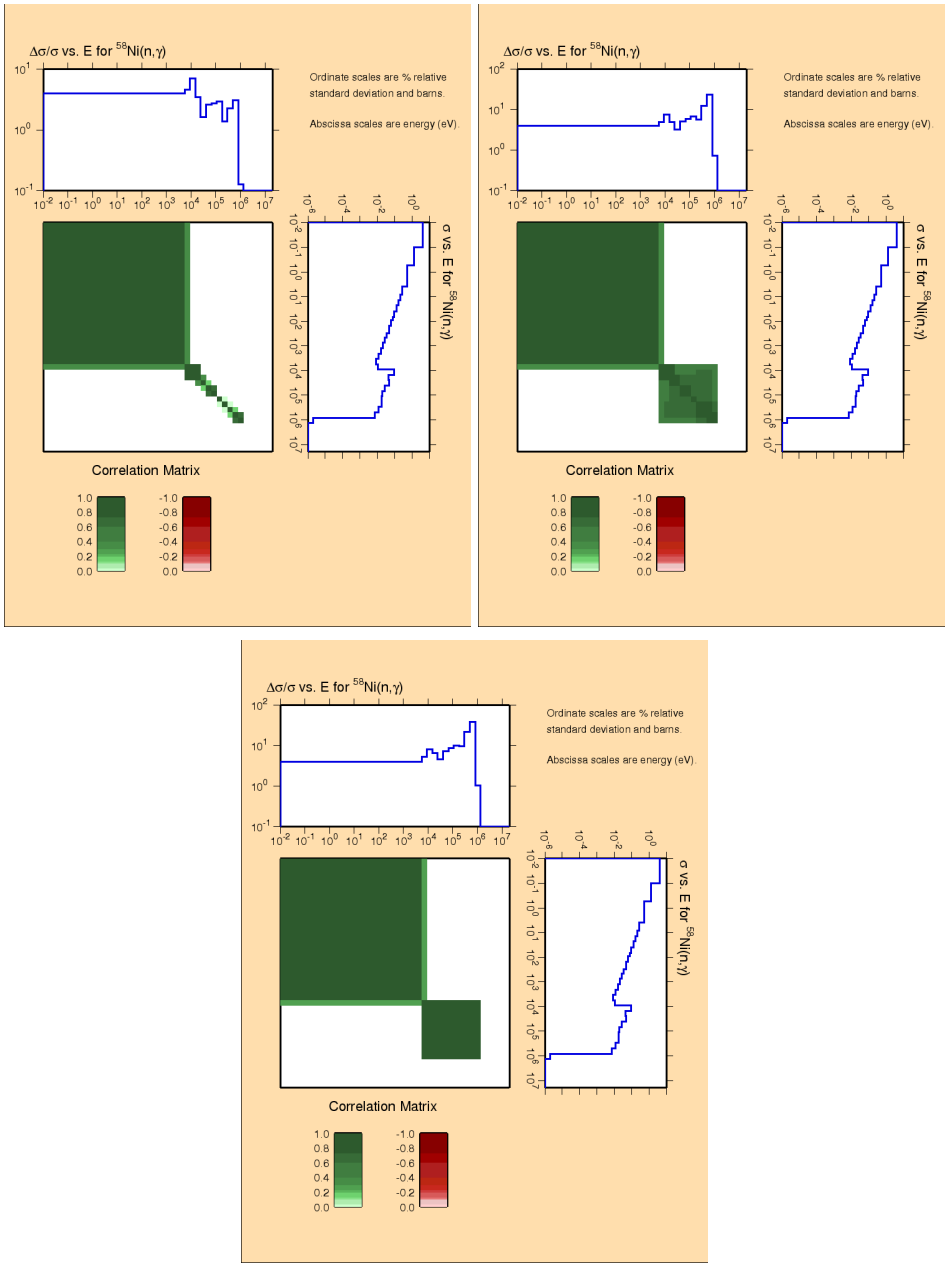

Figure 3.24: Covariances for ^{58}Ni capture in 33-energy groups for three values of resonance-resonance and bin-bin correlation coefficients: 0.0 (top left), 0.5 (adopted, top right) and 1.0 (bottom).

3.4.2 Elastic scattering

Evaluation is again performed in three steps, similar to what was done for ^{52}Cr and ^{56}Fe. First, we determine energy binning and calculate average elastic scattering cross sections in these bins, see Fig. 3.25. Even though the comparison with NJOY values shows limitations of the kernel approximation, the agreement is still sufficient to proceed with covariance estimate. Importantly, one can again see strong contribution of the potential scattering, implying prominent impact of $\Delta R'$ on average elastic scattering cross section uncertainties.

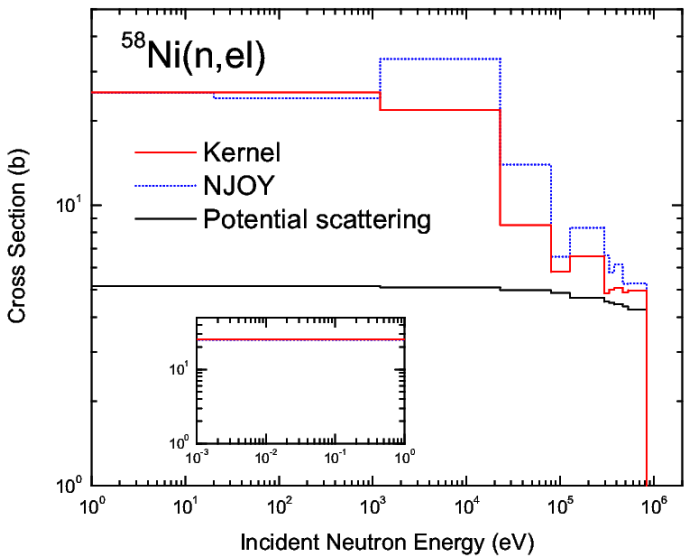

Figure 3.25: Comparison of average cross sections for ^{58}Ni elastic scattering obtained from kernels (above 1 keV) and from NJOY in the whole energy range. The kernel values in the thermal region (below 1keV) were obtained directly from the thermal cross section. Shown in the insert is the energy region from 10^{-3} eV to 10 eV.

As the second step, we computed uncertainties for these average cross sections. Results are shown in Fig. 3.26. As one can see impact of corr(Γ_n, Γ_n) is fairly small, major reason being strong contribution from potential scattering.

Strong contribution to uncertainties from potential scattering is shown in Fig. 3.27. Neglection of this contribution (see $\Delta R' = 0.0$ curve) would lead to completely un-

realistic uncertainties of less than 1%. The 1st bin in the resonance region (1 keV - 20 keV) deserves specific attention. This bin, where potential scattering contributes only about 5 b to full 22 b average cross section, has one very strong neutron resonance, E_0 = 15.3 keV with Γ_n = 1390 ± 10 eV or 0.7%. This means that the cross section uncertainty purely from the resonance term is on the level of (17/22)×0.7% ≈ 0.5%. Thus, even though potential scattering cross section is comparatively small, it enhances the full uncertainty considerably, to about 2.5%.

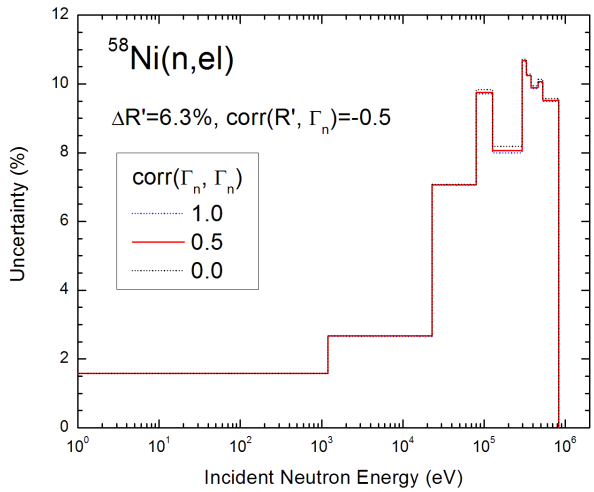

Figure 3.26: Uncertainties of ^{58}Ni(n,el) average cross sections. Shown are results for three values of resonance-resonance correlation coefficients, corr(Γ_n, Γ_n), adopted uniformly for each energy bin. Impact of corr($\Gamma_\gamma, \Gamma_\gamma$) on scattering is marginal.

Finally, we combine these bin uncertainties into full covariance matrix, Fig. 3.28. We adopted default values for correlation coefficients.

3.4.3 Comparison with ENDF/A

We compare our covariances with those produced by Derrien *et al*, ORNL in 2009 [10]. Their file can be found in ENDF/A library which collects candidate evaluations for the forthcoming ENDF/B-VII.1 release. According to brief MT451 description covariances in the resonance region were evaluated using the code SAMMY. The resonance parameter covariance matrix, stored in MF32 file,

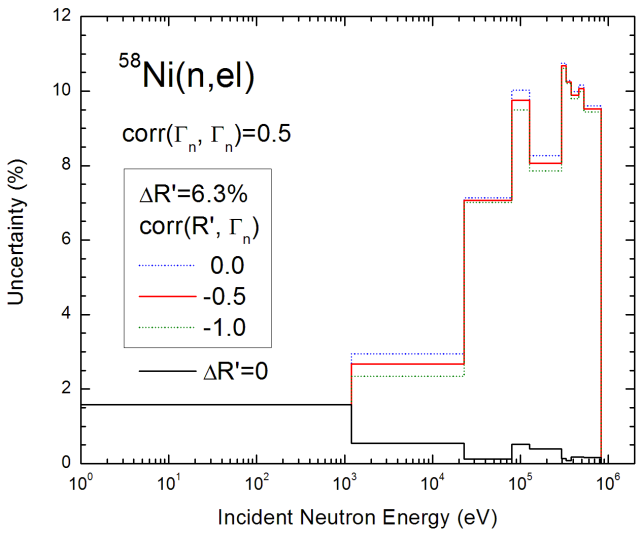

Figure 3.27: Uncertainties of ^{58}Ni(n,el) average cross sections for two values of $\Delta R'$. Used in both cases were default values of corr(Γ_n, Γ_n) = 0.5 and corr(R', Γ_n) = -0.5.

reflects only statistical uncertainties of experimental data. The systematic uncertainties are given in MF33, with 0.5 value for all non-diagonal elements of MF33 correlation matrix.

Comparison of essential features of our covariances and ENDF/A is given in Table 3.8. Considerable differences in capture uncertainties were observed when NJOY processing code was used instead of PUFF. This illustrates continuing deficiencies in processing which should be addressed. We note, however, that elastic scattering uncertainty processed by NJOY and PUFF is in agreement. Since ENDF/A evaluation was done by ORNL we choose to use PUFF results for the present discussion. For both capture and elastic scattering there is agreement in thermal uncertainties. There are, however, also some striking differences. Thus, at the high energy end of the resolved resonance region (812 keV) the uncertainties are entirely different, with ENDF/A claiming much better precision compared to our results.

In the case of ^{58}Ni(n,γ) uncertainty, we have no explanation for the huge broad peak in excess of 20% in ENDF/A in the energy range 10 eV - 10^3 eV. The 1st

Table 3.8: Relative uncertainties of ^{58}Ni+n cross sections obtained in the present work compared with ENDF/A [10]. Uncertainties were obtained from full covariance files by processing with PUFF into 33-group structure.

Reaction	Energy	Uncertainty		Comment
		Present	ENDF/A	
^{58}Ni(n,γ)	Thermal	4%	3.5%	Agreement
	10-10^3 eV	4%	22%	Mistake in ENDF/A?
	600-800 keV	28%	3%	No correlation in ENDF/A?
^{58}Ni(n,el)	Thermal	1.6%	1.8%	Agreement
	10-10^3 eV	2.5%	2%	Agreement
	600-800 keV	9.5%	1.5%	No $\Delta R'$ in ENDF/A

(p-wave) resonance is at E_0 = 6.9 keV and up to about 2 keV capture cross section still duly follows 1/v law. Thus, it is difficult to understand why there should be such a deviation from the thermal uncertainty of 3.5%. We note that ORNL evaluation takes into account fairly strong direct capture which already at the thermal energy contributes considerably to full value of 4.3 b.[3] However, this cannot explain the uncertainty peak either, since direct capture follows 1/v dependence. In the high energy end of the resonance region the capture in ENDF/A does not look realistic. The point is that to reach 3% precision for about 10 mb cross section would be very tough. Observed decline in ENDF/A uncertainties suggests that long-range correlations were likely not taken into account.

In the case of ^{58}Ni(n,el) uncertainty, ENDF/A in the thermal region agrees with our value, but at 600 keV - 800 keV ENDF/A is much lower most likely for not accounting for contribution from the potential scattering. On the other hand, our uncertainties directly depend on the adopted value of $\Delta R'$ which represents only estimate. However, even if we would adopt the lower value, $\Delta R'$ = 3.1%, rather than 6.3%, our uncertainties would still be several times larger than ENDF/A.

[3] According to calculations of ^{58}Ni direct capture at 0.0253 eV by S.F. Mughabghab, σ_γ(direct) = 4.11 b out of 4.49 ± 0.16 b.

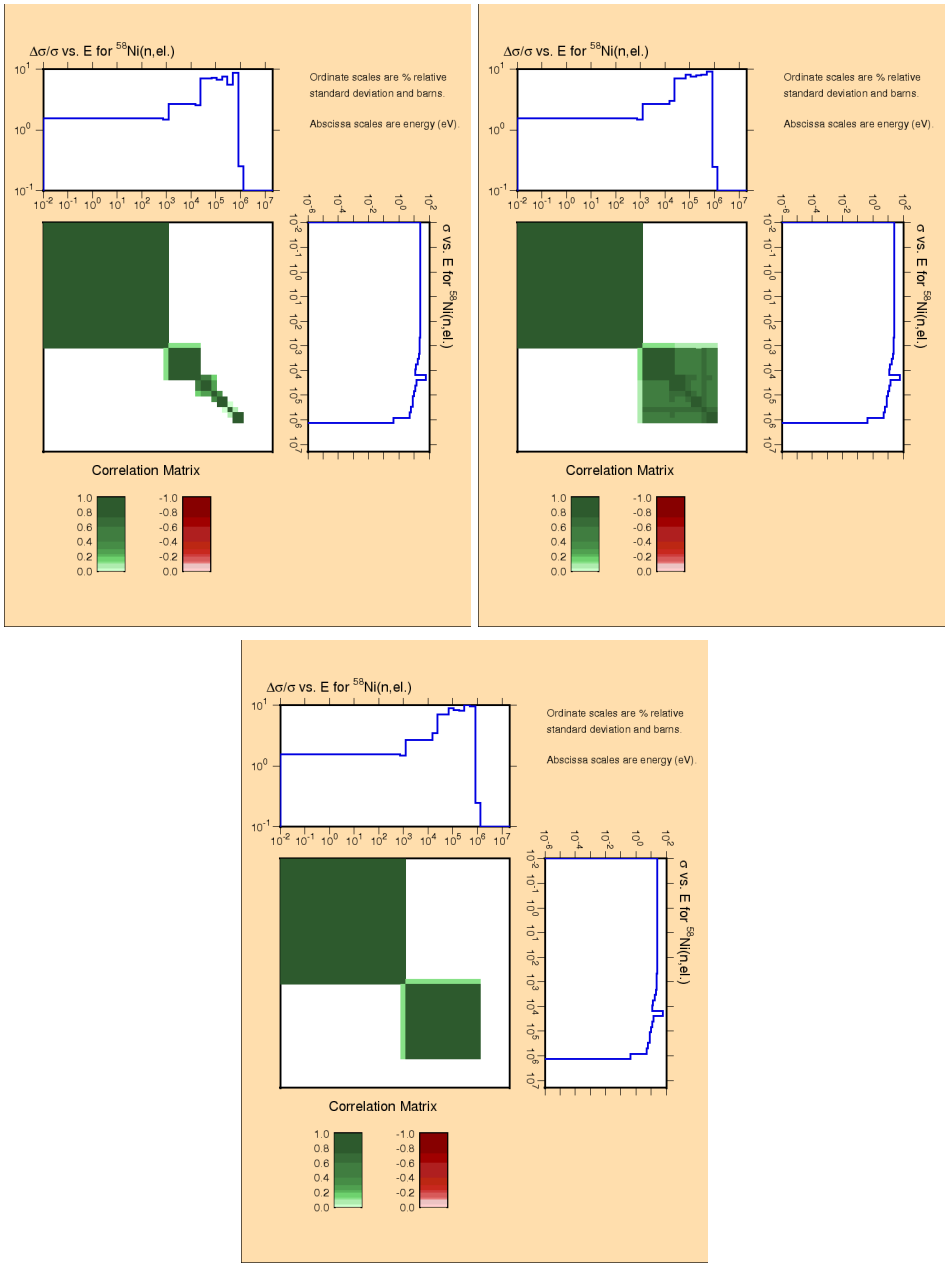

Figure 3.28: Covariances for ^{58}Ni elastic scattering in 33-energy groups for three values of resonance-resonance and bin-bin correlation coefficients: 0.0 (top left), 0.5 (adopted, top right) and 1.0 (bottom).

Chapter 4

Quality assurance

Quality Assurance (QA) of covariances is important aspect of the evaluation process. Our QA procedures address formatting, mathematical properties of covariances matrices, and plausibility of cross section uncertainties.

4.1 Compliance with ENDF-6 format

In the present work we used MF33 format for covariance matrices. This format was implemented in fairly simple and straightforward manner for all three materials under discussion. Covariance matrices are supplied for capture and elastic scattering, they comply with the format as specified in the latest version of ENDF-6 Formats Manual [5].

4.2 Mathematical properties of covariance matrices

This QA test consists of three requirements:

- Symmetry. All our matrices are symmetric,

$$\mathrm{cov}(i, j) = \mathrm{cov}(j, i). \tag{4.1}$$

- Schwarz inequality. Correlation coefficients in each of our matrices are within -1.0 and +1.0 boundaries,

$$-1 \leqq \mathrm{corr}(i, j) \leqq 1. \tag{4.2}$$

- Positive-definiteness. Eigenvalues of our matrices should be either positive or at least semi-positive. This means that after diagonalizing a matrix all diagonal elements (eigenvalues) meet requirement

$$\mathrm{cov}(i, i) \geq 0. \tag{4.3}$$

  We note that the way how we constructed the matrices does not implicitly guarantee their positive-definitiveness. However, the matrices are fairly simple and the fix, if at all necessary, should be also relatively simple with small impact on final results.

4.3 Cross section uncertainties

We apply two QA tests to cross section uncertainties. First, we compare our uncertainties with those of well established integral quantities. Second, we check whether our uncertainties do not fall below certain acceptable limit, the goal being to avoid claims of unrealistic precision of cross sections.

4.3.1 Integral uncertainties

We compare our uncertainties with those of the following integral quantities:

- Thermal values. Suitable for both capture and elastic scattering. Comparison is made with data in Atlas, adjusted for possible differences with cross sections given in ENDF/B-VII.0 library.
- Resonance integrals (capture only). Comparison is made with data in Atlas.
- 30-keV Maxwellian average. Suitable for capture only. Comparison is made with the uncertainties given in KADoNiS library [13]. This is an independent database maintained by the nuclear astrophysics community, not influenced by links to traditional nuclear data evaluation projects.

Summary of the integral uncertainty testing for ^{52}Cr, ^{56}Fe and ^{58}Ni is given in Table 4.1. In the thermal region our uncertainties either agree with Atlas or are more conservative since we had to account for differences with cross sections in ENDF/B-VII.0 library. Shown for the record in Table 4.2 is similar comparison for ^{55}Mn using the results of our previous work [1].

Table 4.1: Comparison of uncertainties for capture and elastic scattering cross sections for 3 major structural materials. Values obtained in this work are compared with the uncertainties of integral quantities in Atlas [4] and KADoNiS library [13]. Given in brackets are absolute values of cross sections.

Reaction	Thermal		Res. Int.		30-keV Maxwellian		
	This work[a]	Atlas	This work[b]	Atlas	This work[c]	KADoNiS	Atlas
^{52}Cr(n,γ)	3.0%	2.3%	3.0%	6%[+)]	8.6% (8.7mb)	26% (8.8mb)	23% (9.1mb)
(n,el)	2.5%	0.7%					
^{56}Fe(n,γ)	5.4%	5.4%	5.4%	11%	7.9% (11.5mb)	4.3% (11.7mb)	8.6% (15.1mb)
(n,el)	4.0%	3.9%					
^{58}Ni(n,γ)	4.0%	2.3%	4.0%	9.5%	4.5% (39.9mb)	3.9% (38.7mb)	6.2% (40.2mb)
(n,el)	1.6%	1.6%					

a) See Table 3.5 for explanation of differences between this work and Atlas.

b) Computed by NJOY using MF33 grid in GROUPR.

c) Computed by NJOY using MF33 grid. Cross sections refer to ENDF/B-VII.0.

[+)] No value is given in Atlas; estimated by PO in July 2010.

Table 4.2: Comparison of our uncertainties for ^{55}Mn(n,γ) and (n,el) [1] with the uncertainties of integral quantities [4, 13]. Given in brackets are also cross sections for 30-keV Maxwellian spectrum.

Reaction	Thermal		Resonance Int.		30-keV Maxwellian	
	Our	Atlas	Our	Atlas	Our	KADoNiS
^{55}Mn(n,γ)	0.8%	0.37%	3.3%	3.7%	10% (31.0 mb)	7.5% (39.6 mb)
(n,el)	3.0%	1.5%				

For structural materials resonance integrals in Atlas are available for capture only (for actinides also fission resonance integrals). Related uncertainties based

on data of this work were computed by NJOY using our original MF33 energy grid in GROUPR. These uncertainties can be also estimated as follows. Resonance integrals are defined as [4]

$$RI_\gamma = \int_{0.5eV}^{\infty} \frac{1}{E}\sigma_\gamma(E)dE \tag{4.4}$$

which can be approximated by restricting the upper energy to a lower energy, such as 100 keV adopted by JEFF-3 project. Then,

$$RI_\gamma \approx \int_{0.5eV}^{100keV} \frac{1}{E}\sigma_\gamma(E)dE \approx \bar{\sigma}_\gamma \times \ln(10^5/0.5),$$

where $\bar{\sigma}_\gamma$ is the average capture cross section computed by NJOY for 1/E flux and $\ln(10^5/0.5) = 12.2$ is the neutron lethargy. Taking into account 1/E weighting function and strong decline of capture cross sections for all materials under discussion, one can neglect contributions from above 1 keV. Below this energy we treated covariances with the thermal region approach, therefore, relative uncertainty

$$\Delta RI_\gamma \approx \Delta\sigma_\gamma(E_{th}).$$

Atlas provides no capture RI uncertainty for ^{52}Cr. For ^{56}Fe and ^{58}Ni our results are lower than Atlas by more than a factor of two. *This issue will be addressed by refining our procedure, see Chapter 5, page 64.*

Comparison with 30-keV Maxwellian averages can be done for capture for all three materials. One can see that our performance is mixed: ^{52}Cr uncertainty is considerably smaller than KADoNiS, ^{56}Fe exceeds KADoNiS almost by a factor of two, and ^{58}Ni is in good agreement.

4.3.2 Minimal uncertainties

We adopted criterion that uncertainties in the 33-group representation should be larger than reasonable minimal values, which we set to 2%. We require that

- $\Delta\sigma(n,\gamma) > 2\%$,
- $\Delta\sigma(n,el) > 2\%$.

These minimal values take into account the fact that to reach 2% precision in neutron cross section measurements is indeed very tough. Precision better than 2%

has been achieved in determining the best established cross sections of neutron standards.

We checked all uncertainties and made sure that if precision better than 2% is claimed, then plausible explanation is available. This test produced warning only once, for ^{58}Ni(n,el) in the thermal region. There, we adopted 1.6% value given in Atlas, taking into account good agreement with the thermal cross section in ENDF/B-VII.0.

4.4 Dispersion analysis

The above QA tests do not asses plausibility of our results in full. Thus, for capture the tests probe low energies, leaving open an assessment of large uncertainties at the high end of the resonance region. QA tests for elastic scattering probe the thermal region only. In view of this, we reviewed also central values in major libraries with the idea to get collective opinion of the nuclear data community on these cross sections. Dispersion between the libraries can be indicative of uncertainties associated with these data.

4.4.1 Capture

Average capture cross sections for ^{52}Cr, ^{56}Fe and ^{58}Ni are summarized in Table 4.3. Large dispersions seen for ^{52}Cr and ^{56}Fe support our uncertainties. However, dispersion for ^{58}Ni is only 10%, suggesting that our uncertainty of 27% at the end of the resonance region is probably too conservative.

Table 4.3: Comparison of average capture cross sections for ^{52}Cr, ^{56}Fe and ^{58}Ni in recent releases of major data libraries. Averages are computed for the highest 500 keV energy bin. Differences to ENDF/B-VII.0 are shown in the last column, with uncertainties of the present work given in brackets.

Reaction	Energy keV	Library	Year	$\overline{\sigma}_\gamma$ mb	Diff
^{52}Cr(n,γ)	500-1000	ENDF/B-VII.0	2006	2.50	(31%)
		ENDF/A	2009	2.18	-13%
		JENDL-4.0	2010	2.18	-13%
		ROSFOND	2008	1.70	-32%
		JEFF-3.1	2005	1.70	-32%
^{56}Fe(n,γ)	350-850	ENDF/B-VII.0	2006	5.88	(28%)
		ENDF/A	n/a	n/a	n/a
		JENDL-4.0	2010	5.90	0%
		ROSFOND	2008	6.52	+11%
		JEFF-3.1	2005	3.68	-37%
^{58}Ni(n,γ)	300-800	ENDF/B-VII.0	2006	10.3	(27%)
		ENDF/A	2009	9.3	-10%
		JENDL-4.0	2010	10.3	0%
		ROSFOND	2008	10.3	0%
		JEFF-3.1	2005	10.3	0%

4.4.2 Elastic scattering

Average elastic scattering cross sections for ^{52}Cr, ^{56}Fe and ^{58}Ni are summarized in Table 4.4. Large dispersion is seen only for ^{52}Cr, while dispersion for ^{56}Fe and ^{58}Ni is small. Even though we show the averages over the entire resonance region, they pretty reasonably reflect the situation for smaller binning as well.

Table 4.4: Comparison of average elastic scattering cross sections in major data libraries. Averages are computed for the whole resonance region which grasp the situation also if smaller bins were used. Shown in the last column are differences to ENDF/B-VII.0, with uncertainties of the present work valid for the highest 500 keV bin given in brackets.

Reaction	Energy keV	Library	Year	$\bar{\sigma}_n$ b	Diff
^{52}Cr(n, el)	1-1000	ENDF/B-VII.0	2006	3.74	(16%)
		ENDF/A	2009	3.28	-12%
		JENDL-4.0	2010	3.28	-12%
		ROSFOND	2008	3.44	-8%
		JEFF-3.1	2005	3.44	-8%
		CENDL-3.1	2010	3.85	+2%
^{56}Fe(n, el)	1-850	ENDF/B-VII.0	2006	3.73	(14-16%)
		ENDF/A	n/a	n/a	n/a
		JENDL-4.0	2010	3.73	0%
		ROSFOND	2008	3.75	+0.5%
		JEFF-3.1	2005	3.75	+0.5%
^{58}Ni(n, el)	1-800	ENDF/B-VII.0	2006	5.54	(9-10%)
		ENDF/A	2009	5.55	0%
		JENDL-4.0	2010	5.54	0%
		ROSFOND	2008	5.54	0%
		JEFF-3.1	2005	5.54	0%

4.5 Optical model prediction for ^{56}Fe(n,tot)

It is instructive to look into optical model predictions for neutron elastic scattering. This might help us with assessing plausibility of our uncertainties. In a recent study by Pigni *et al* [14] minima in cross section uncertainties predicted by optical model were studied to considerable detail using ^{56}Fe as illustrative example.

Several observations can be made for ^{56}Fe. First, the resonance capture is very weak. Therefore, total cross sections are essentially identical with elastic scattering cross sections. Second, optical model predicts smooth cross sections averaged over strongly fluctuating resonances. This can be seen on ^{56}Fe(n,tot) cross sections shown in Fig. 4.1. We note that fluctuations of ENDF/B-VII.0 data continue well above the resolved resonance region.

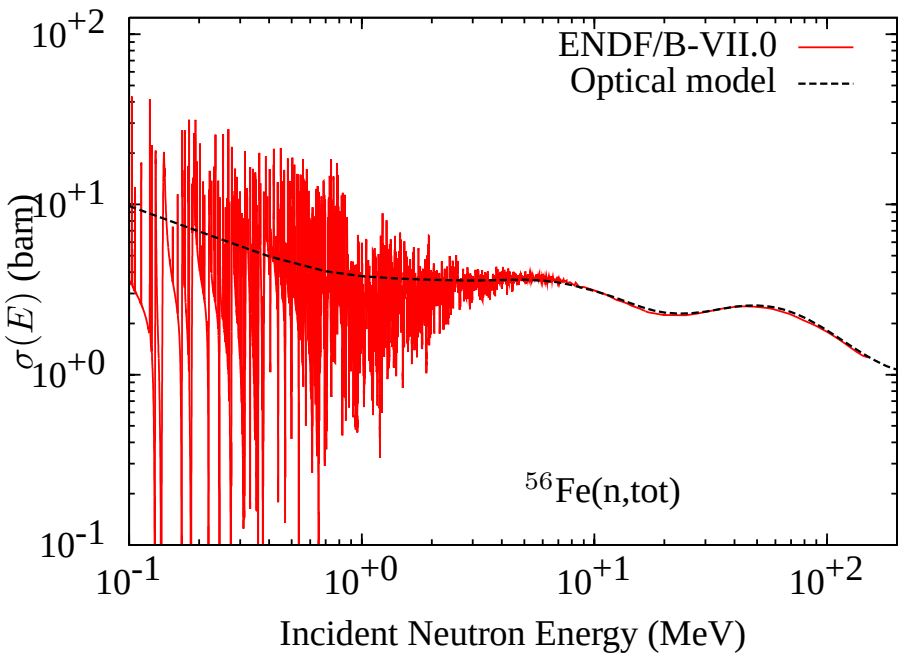

Figure 4.1: ^{56}Fe(n,tot) cross sections: optical model values for Koning-Delaroche potential are compared with fluctuating structure of neutron resonances. Figure was taken from M. Pigni *et al* [14].

Related ^{56}Fe(n,tot) cross section uncertainties are shown in Fig. 4.2. Use was

made of several typical optical model potential parametrizations. Parameter uncertainties were taken from the recently released RIPL-3 library [15].

Of most interest to the present work is the energy region 0.1 MeV - 0.85 MeV. One can see that in this energy range optical model predicts uncertainties between about 5-10%. Certain reduction of these values should be expected if correlations between optical model parameters were included. This suggests that ^{56}Fe(n,el) uncertainties of our initial estimate shown in Figs. 3.17 and 3.18 on page 43 are too high. This in turn suggests that our estimate of $\Delta R'$ in the resonance region is too conservative and should be reduced.

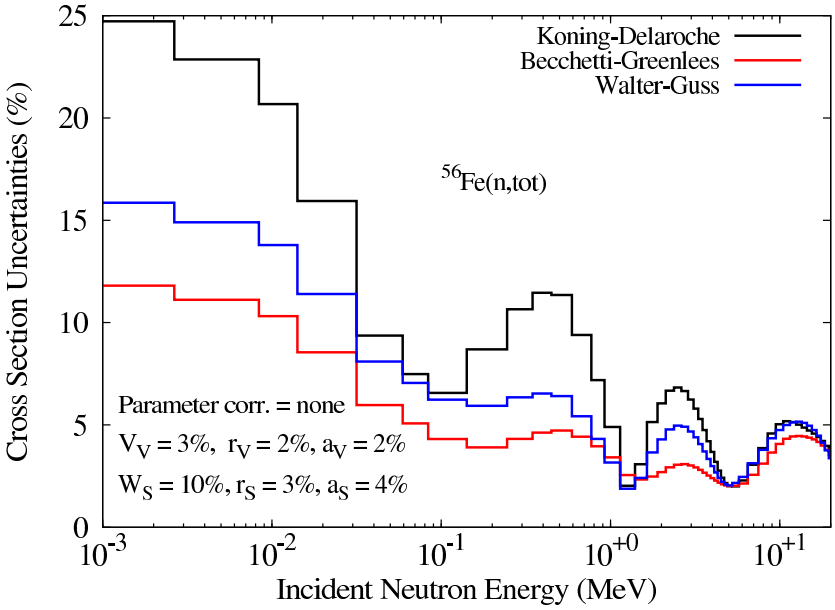

Figure 4.2: ^{56}Fe(n,tot) cross section uncertainties: optical model predictions using different sets of OM parameters with parameter uncertainties taken from RIPL-3 library. Figure was taken from M. Pigni *et al* [14].

Chapter 5

Refinements in evaluation procedure

QA testing revealed several issues which we attempted to resolve by refining our evaluation procedure.

5.1 Modification of default values

The following issues were addressed and changes in default values were made:

1. Capture resonance integral (RI) uncertainties. Refinement applies to the thermal energy region. One should use uncertainty of $\Delta\sigma(E_{th})$ up to 0.5 eV only. For higher energies in the thermal region, 0.5 eV - 1 keV for materials discussed here, one should adopt ΔRI_γ. Thus,

$$\Delta\sigma_\gamma(E) = \Delta\sigma_\gamma(E_{th}) \quad \text{for} \quad E < 0.5\ eV \tag{5.1}$$

and

$$\Delta\sigma_\gamma(E) = \Delta RI_\gamma \quad \text{for} \quad E > 0.5\ eV. \tag{5.2}$$

This refinement would lead to much better agreement with resonance integral uncertainties of Atlas of Neutron Resonances.

2. Scattering radius uncertainty. Our initial default estimate enhanced thermal uncertainty by a factor of two. This should be reduced to a factor of 1.5,

$$\Delta R'(E_{\text{res}}) = k_{R'}\Delta R'(E_{\text{th}}), \tag{5.3}$$

where default value of the multiplier is

$$k_{R'} = 1.5. \tag{5.4}$$

This refinement would reduce our estimate of elastic scattering uncertainties which seemed to be too conservative when a factor of two was used.

3. Capture uncertainties at higher energies[1]. Dispersion analysis indicated certain overestimation of uncertainties. This issue can be addressed by using lower values for correlation coefficients, $\mathrm{corr}(\Gamma_\gamma, \Gamma_\gamma)$. Our default should be selected in such a way that resulting cross section uncertainties should reach middle values. This differs with the current approach, where $\mathrm{corr}(\Gamma_\gamma, \Gamma_\gamma)$ is chosen to reach the middle value (0.5 on the scale 0.0-1.0). Thus,

$$\mathrm{corr}(\Gamma_\gamma, \Gamma_\gamma)$$

should be selected so that

$$\Delta\sigma_n(\mathrm{corr}) \approx \frac{1}{2}\{\Delta\sigma_n(\mathrm{corr} = 0) + \Delta\sigma_n(\mathrm{corr} = 1)\} \tag{5.5}$$

This refinement would more evenly project our lack of knowledge about correlation coefficients.

5.2 Specific changes for ^{52}Cr, ^{56}Fe and ^{58}Ni

In addition to modification of default values, several specific changes for individual materials attempt to address some remaining issues identified by QA tests.

^{52}Cr. Capture uncertainties in the energy range around 30 keV might be enhanced by a factor of two to bring our 30-keV Maxwellian average closer to KADoNiS[2].

^{56}Fe. Dispersion analysis shows that for ^{56}Fe(n,el) cross sections there relatively small differences between recent releases of major data libraries. This

[1] This change in high energy capture uncertainties was considered but not implemented

[2] This change in ^{52}Cr capture uncertainties in 30-keV range was considered, but not implemented

suggests that our estimate of $\Delta R'(E_{\rm res})$ is too conservative. In view of this we reduced the multiplier in Eq. (5.4) to the lowest possible value,

$$k_{R'}(^{56}Fe) = 1.0.$$

^{58}**Ni**. Dispersion analysis shows that for ^{58}Ni(n,el) there small differences between major data libraries. This suggests that our estimate of $\Delta R'(E_{\rm res})$ is too conservative. In view of this we reduced the multiplier in Eq. (5.4) to the lowest possible value,

$$k_{R'}(^{58}Ni) = 1.0.$$

5.3 Summary of adopted input uncertainties

For the record in Table 5.1 we summarize adopted input uncertainties for various quantities of interest.

Table 5.1: Summary of adopted uncertainties, $\Delta\sigma_\gamma$, $\Delta\sigma_n$ in the thermal region and $\Delta R'(E_{\rm res})$. Also given are input quantities for Eq. (5.4), R' and $\Delta R'(E_{\rm th})$ in units of fm, and multiplier $k_{R'}$.

Reaction	$\Delta\sigma$, thermal below 0.5 eV	above 0.5 eV	$\Delta R'(E_{\rm res})$ Input R'	$\Delta R'$	$k_{R'}$	Value	Comment
^{52}Cr (n,γ)	3.0%	6.0%					ΔRI_γ estimated
(n,el)	2.5%		5.4	0.3	1.5	8.3%	
^{56}Fe (n,γ)	5.4%	11%					
(n,el)	4.0%		5.9	0.3	1.0	5.1%	
^{58}Ni (n,γ)	4.0%	9.5%					
(n,el)	1.6%		6.4	0.2	1.0	3.1%	

Chapter 6

Final results

The above modifications were implemented into evaluation procedure, ^{52}Cr, ^{56}Fe and ^{58}Ni evaluations were updated and final results were produced.

6.1 ^{52}Cr final results

Shown below are plots with final results, first for ^{52}Cr(n,γ), then for ^{52}Cr(n,el). Plots for average cross sections remained unchanged and they are not shown.

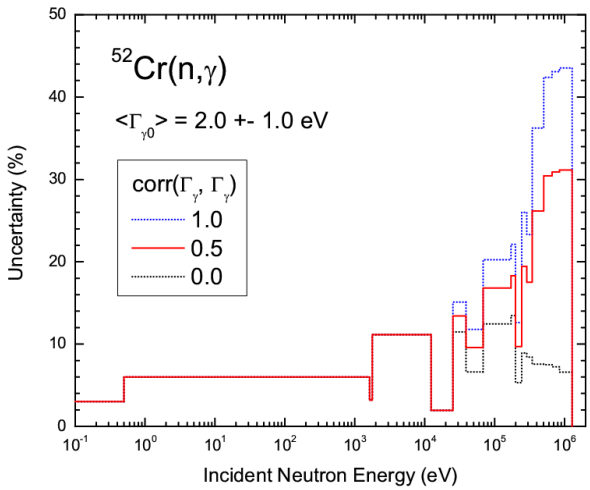

Figure 6.1: ^{52}Cr(n,γ) uncertainties.

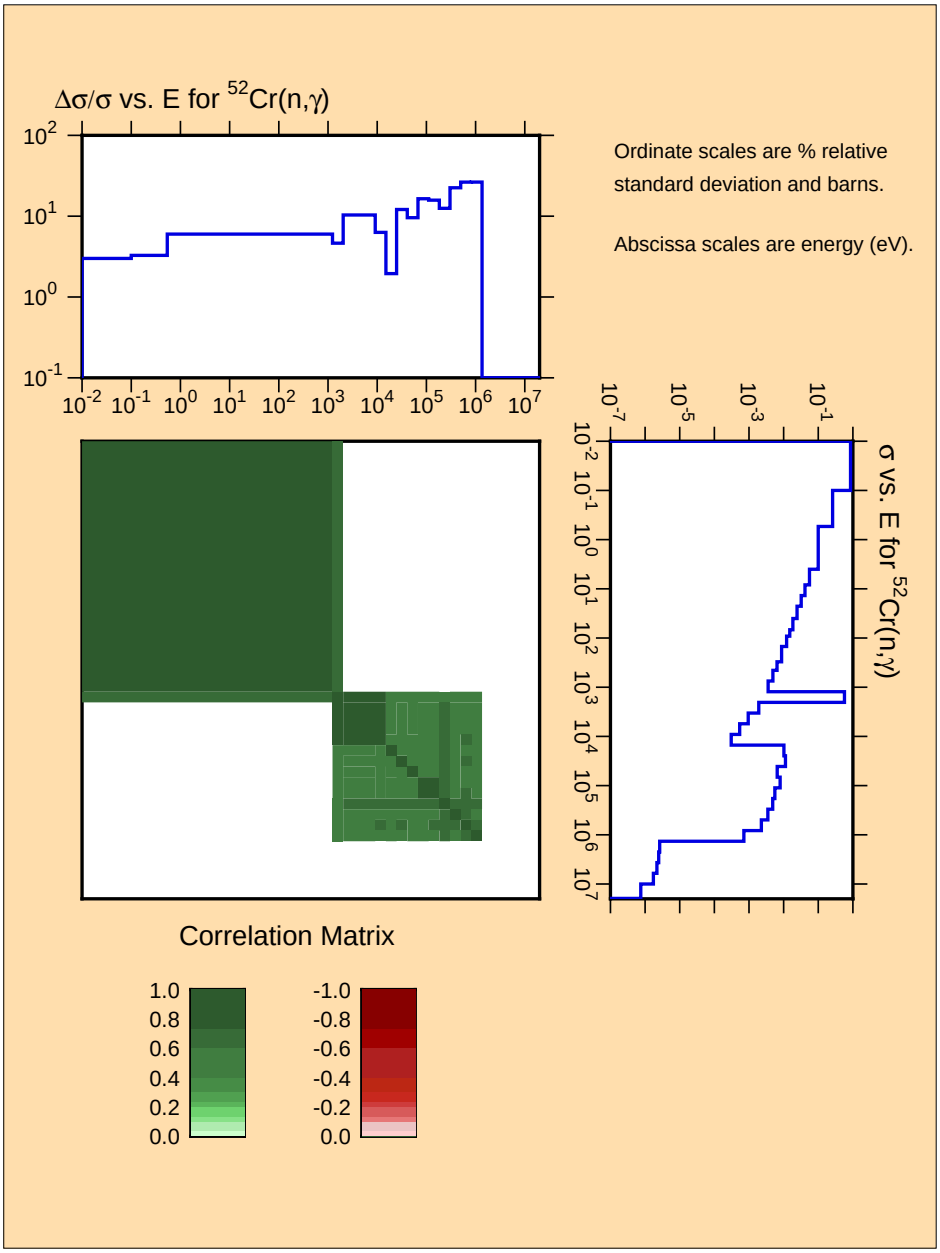

Figure 6.2: ^{52}Cr(n,γ) covariances for adopted values of resonance-resonance as well as bin-bin correlation coefficients, corr = 0.5.

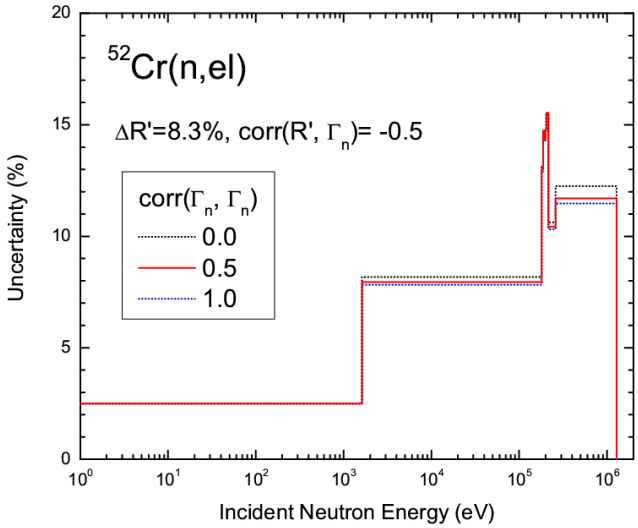

Figure 6.3: ^{52}Cr(n,el) uncertainties: role of corr(Γ_n, Γ_n).

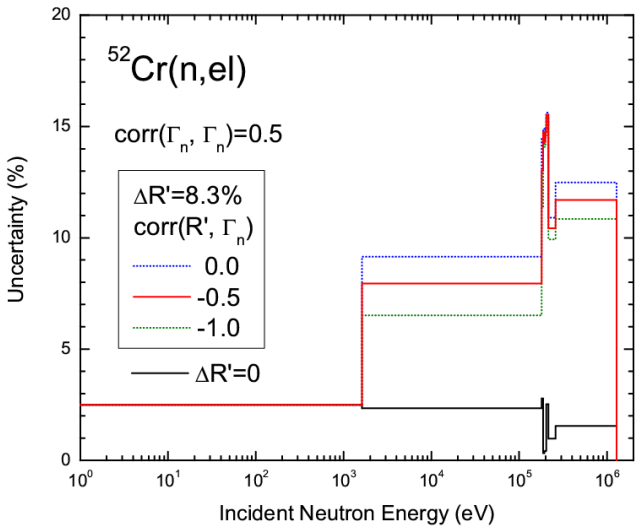

Figure 6.4: ^{52}Cr(n,el) uncertainties: role of corr(R', Γ_n) and impact of $\Delta R'$.

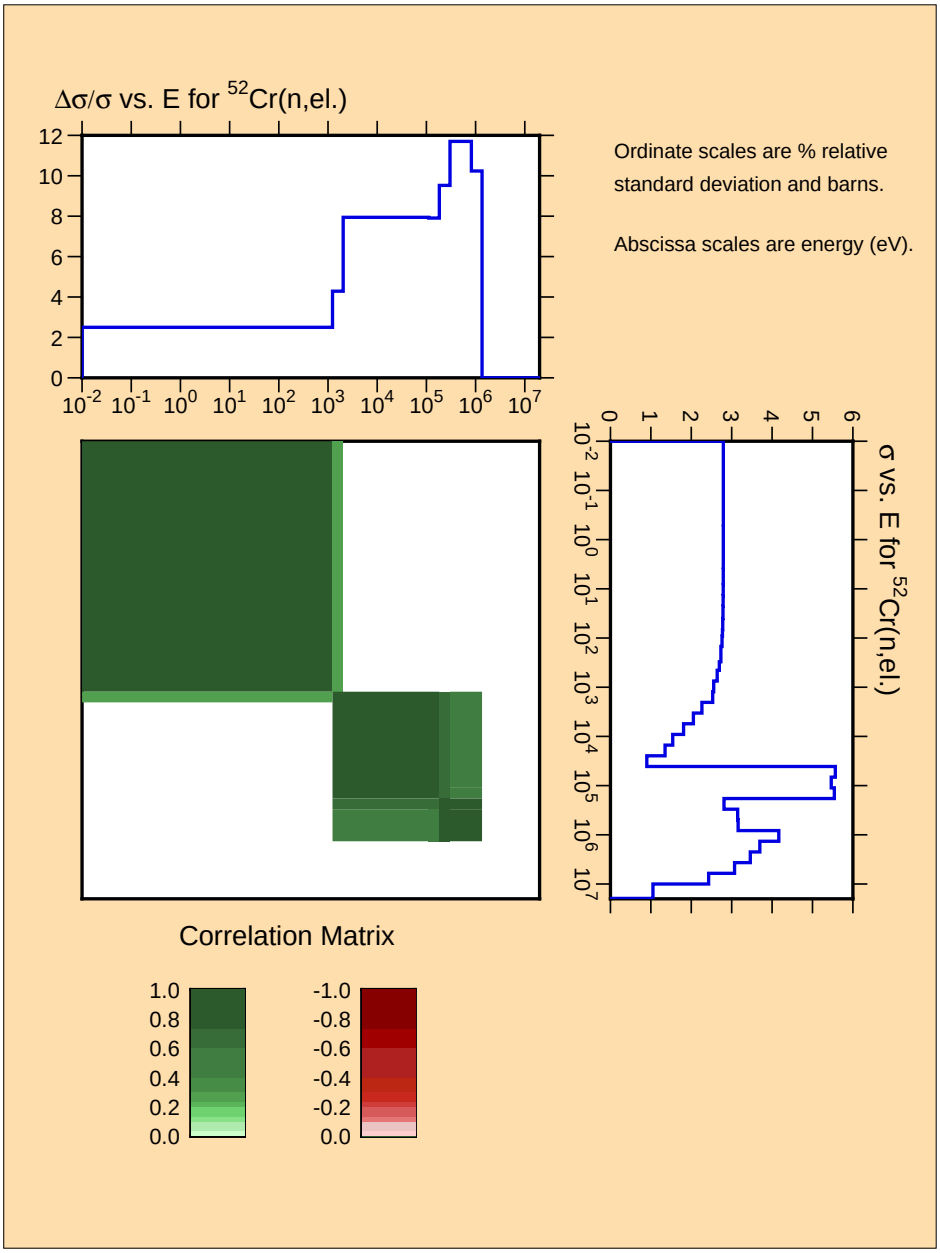

Figure 6.5: ^{52}Cr(n,el) covariances for adopted values of resonance-resonance as well as bin-bin correlation coefficients, corr = 0.5.

6.2 ^{56}Fe final results

Shown below are plots with final results, first for ^{56}Fe(n,γ), then for ^{56}Fe(n,el). Plots for average cross sections remained unchanged and they are not shown.

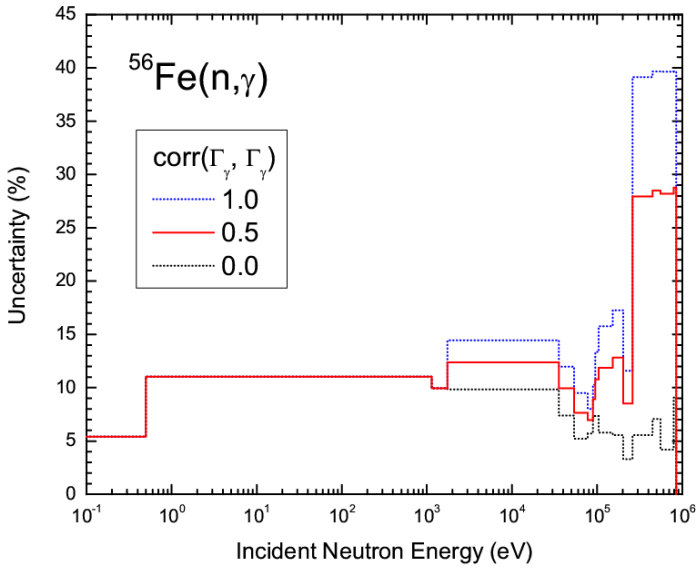

Figure 6.6: ^{56}Fe(n,γ) uncertainties. The only difference compared to Fig. 3.14, p. 40 is enhanced uncertainty in the thermal region just above 0.5 eV, where $\Delta RI_\gamma = 11\%$ rather than $\Delta\sigma(E_{\text{th}}) = 5.4\%$ was used.

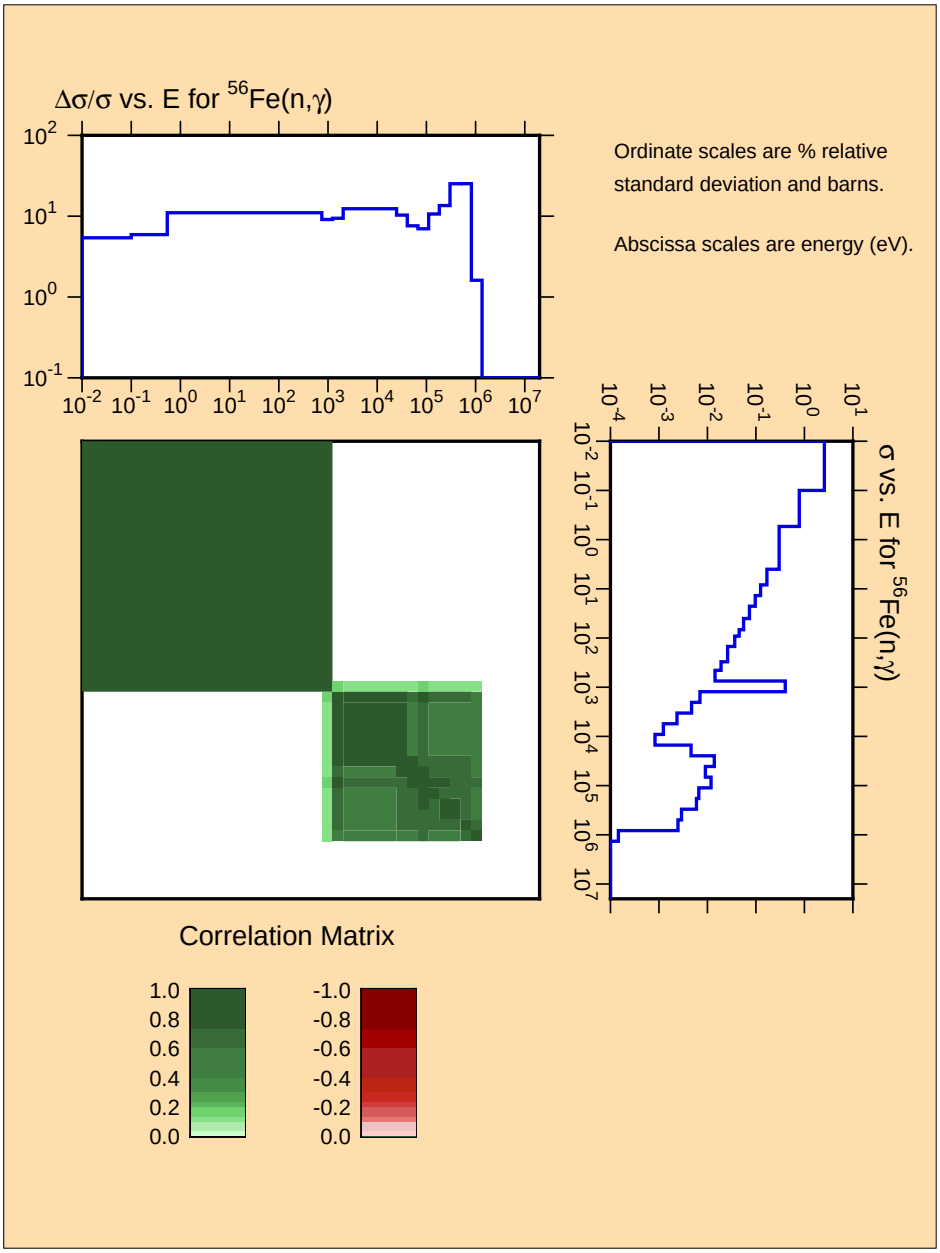

Figure 6.7: ^{56}Fe(n,γ) covariances for adopted values of resonance-resonance as well as bin-bin correlation coefficients, corr = 0.5.

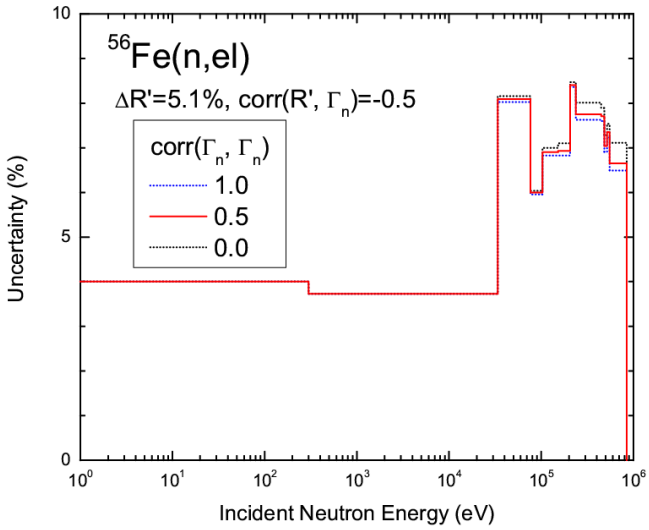

Figure 6.8: ^{56}Fe(n,el) uncertainties: role of corr(Γ_n, Γ_n).

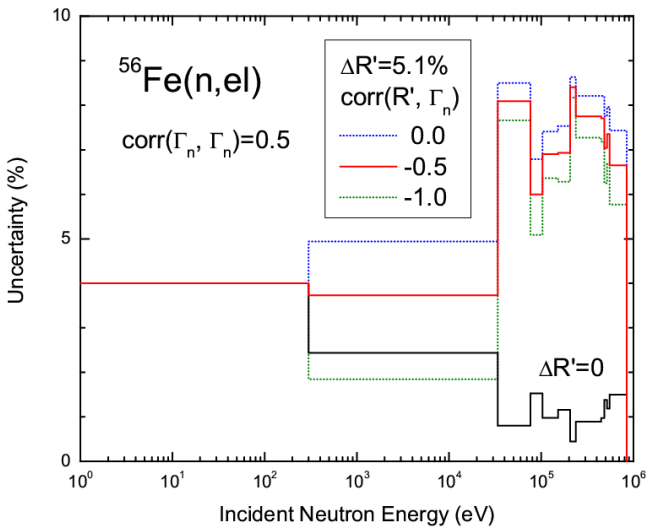

Figure 6.9: ^{56}Fe(n,el) uncertainties: role of corr(R', Γ_n) and impact of $\Delta R'$.

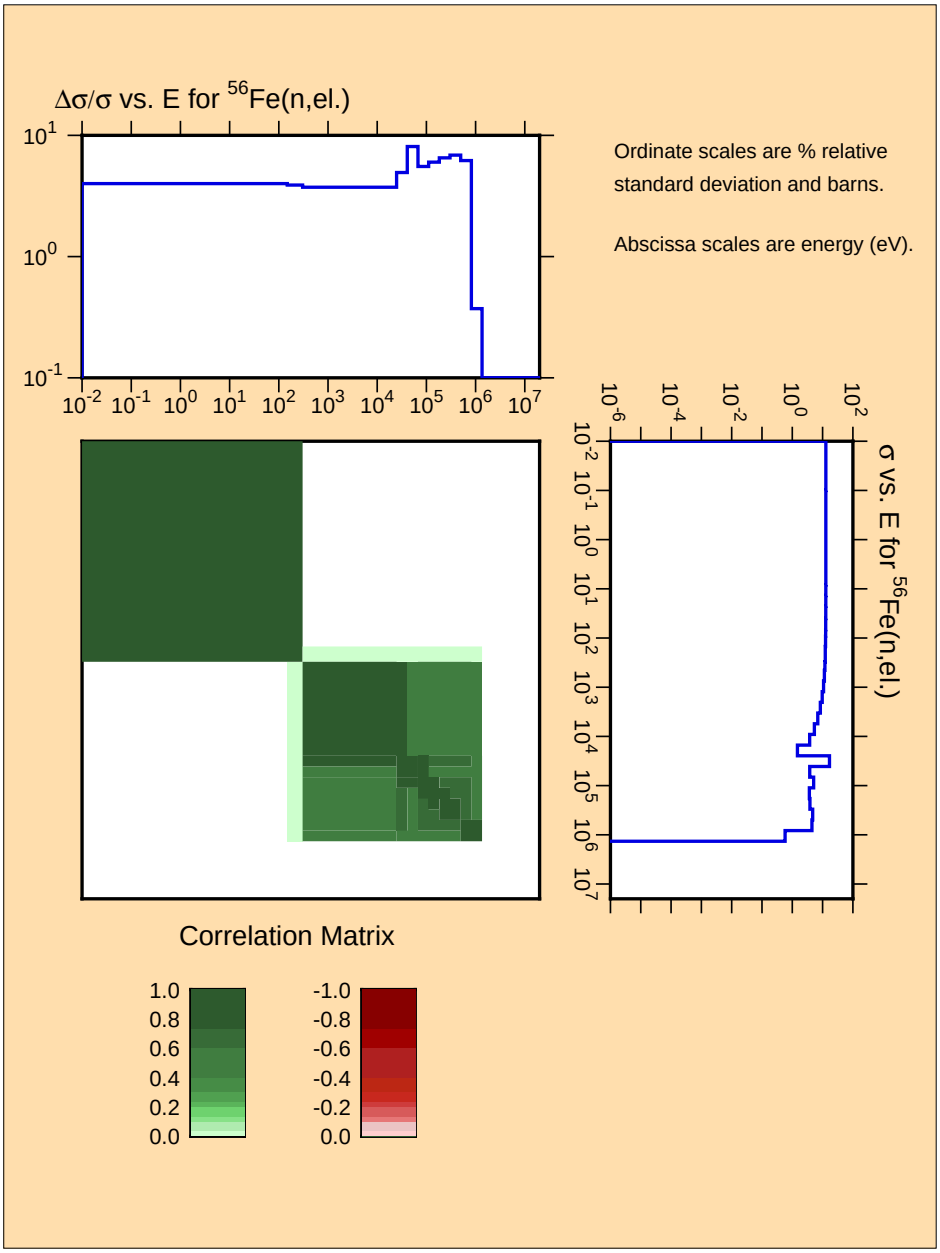

Figure 6.10: ^{56}Fe(n,el) covariances for adopted values of resonance-resonances as well as bin-bin correlation coefficients, corr = 0.5.

6.3 ^{58}Ni final results

Shown below are plots with final results, first for ^{58}Ni(n,γ), then for ^{58}Ni(n,el). Plots for average cross sections remained unchanged and they are not shown.

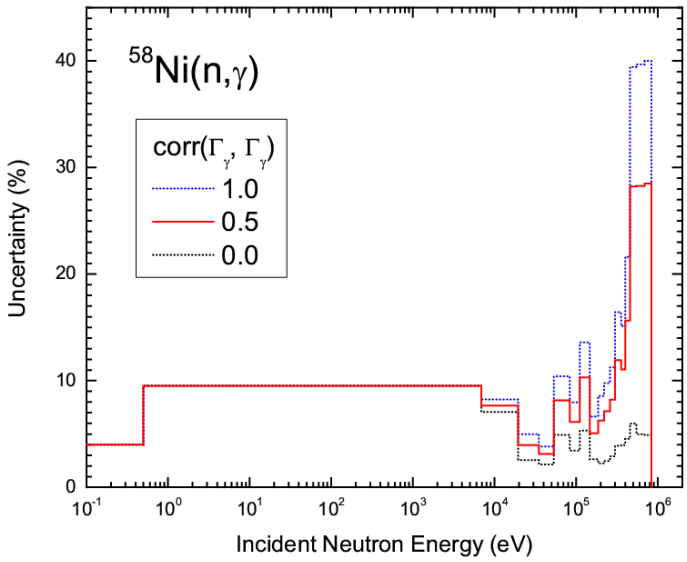

Figure 6.11: ^{58}Ni(n,γ) uncertainties.he only difference compared to Fig. 3.23, p. 48 is enhanced uncertainty in the thermal region just above 0.5 eV, where ΔRI_γ = 9.5% rather than $\Delta\sigma(E_{\text{th}})$ = 4.0% was used.

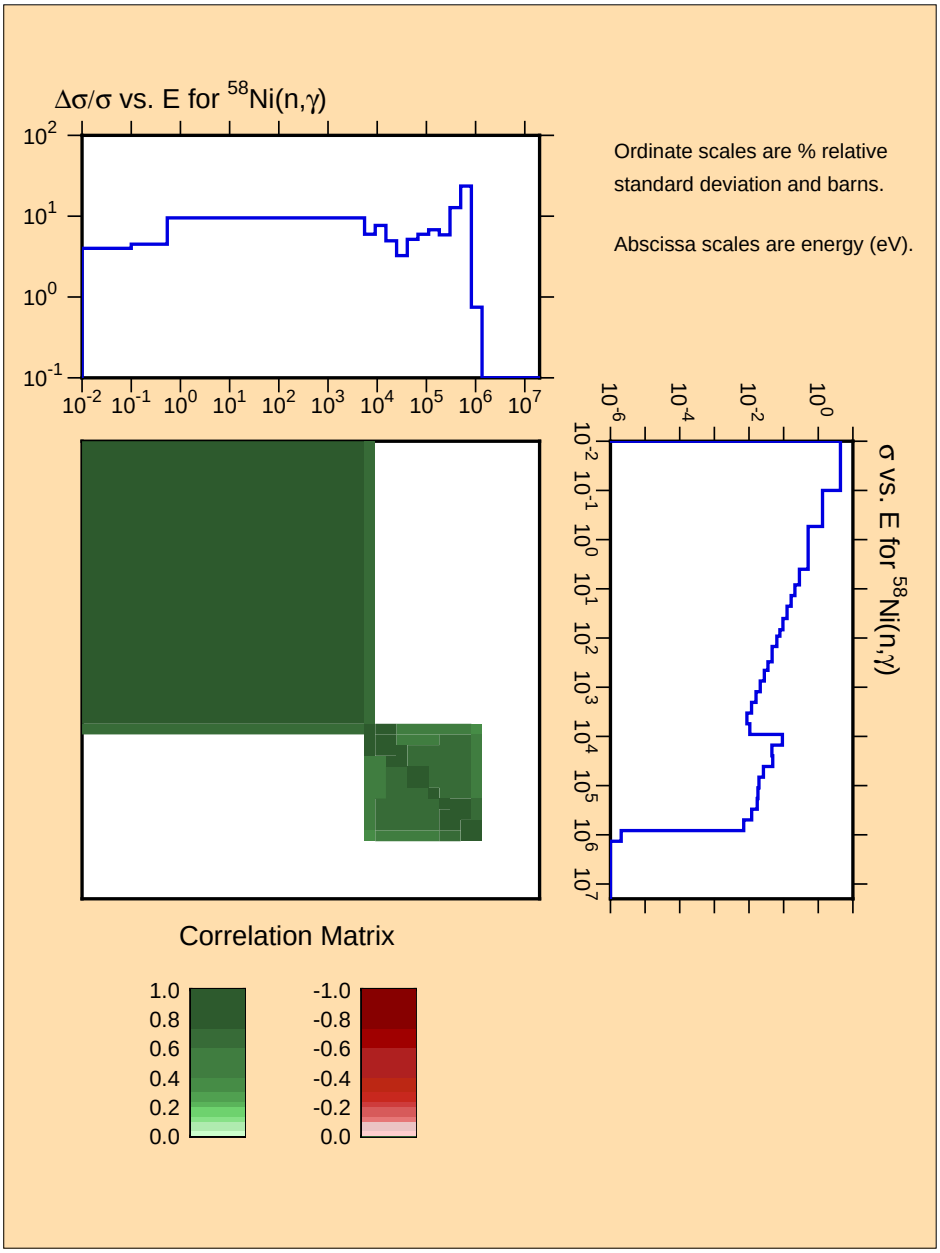

Figure 6.12: ^{58}Ni(n,γ) covariances for adopted values of resonance-resonance as well as bin-bin correlation coefficients, corr = 0.5.

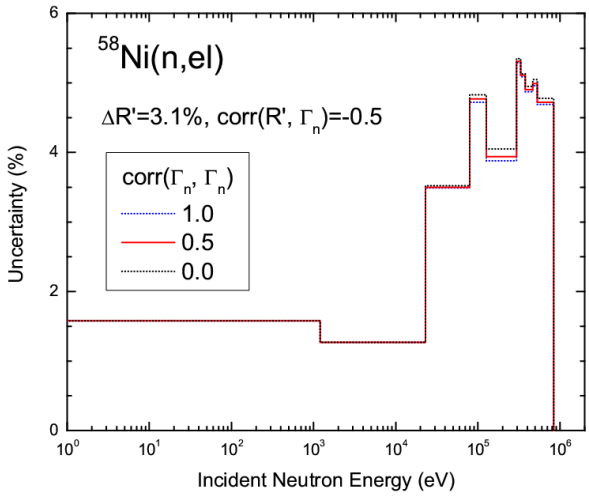

Figure 6.13: ^{58}Ni(n,el) uncertainties: role of corr(Γ_n, Γ_n).

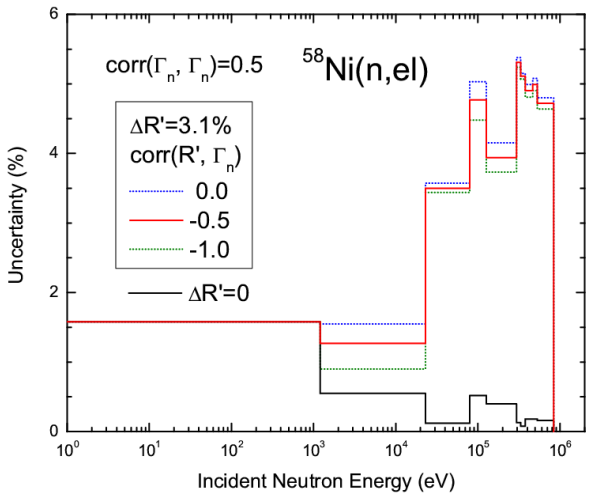

Figure 6.14: ^{58}Ni(n,el) uncertainties: role of corr(R', Γ_n) and impact of $\Delta R'$.

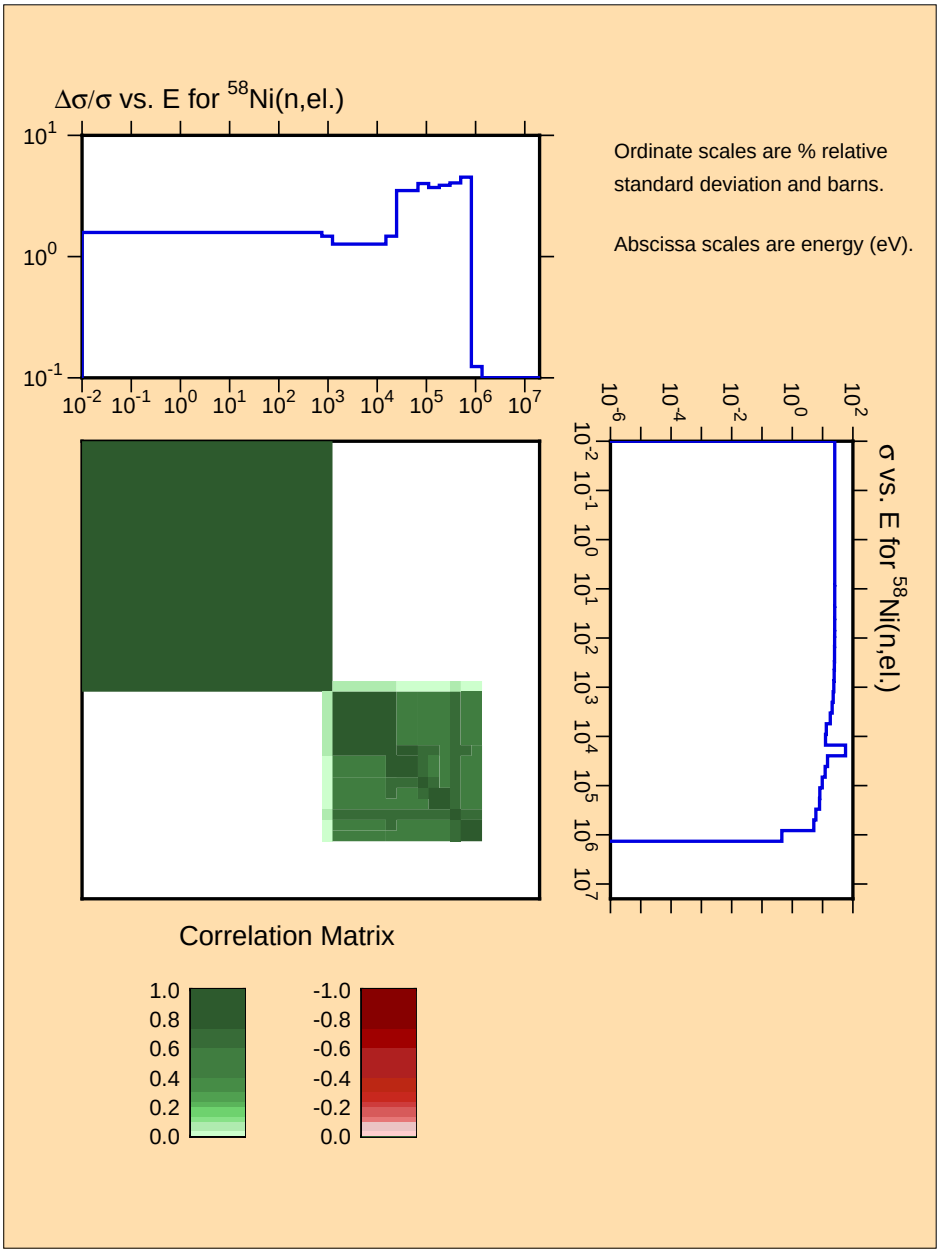

Figure 6.15: ^{58}Ni(n,el) covariances for adopted values of resonance-resonance as well as bin-bin correlation coefficients, corr = 0.5.

6.4 QA of final results

Quality Assurance of final results was done for completeness. All QA criteria discussed in Chapter 4, p. 55 were met as before. The only difference is in uncertainties of integral quantities. These are given in Table 6.1. As expected excellent agreement was obtained for capture RI uncertainties.

Table 6.1: Comparison of uncertainties for capture and elastic scattering cross sections for three major structural materials. Values obtained in this work are compared with the uncertainties of integral quantities in Atlas [4] and KADoNiS library [13]. Given in brackets are absolute values of cross sections.

Reaction	Thermal		Resonance Int.		30-keV Maxwellian	
	This work[a]	Atlas	This work[b]	Atlas	This work[c]	KADoNiS
^{52}Cr(n,γ)	3.0%	2.3%	6%	6%$^{+)}$	8.6% (8.7 mb)	26% (8.8 mb)
(n,el)	2.5%	0.7%				
^{56}Fe(n,γ)	5.4%	5.4%	11%	11%	7.9% (11.5 mb)	4.3% (11.7 mb)
(n,el)	4.0%	3.9%				
^{58}Ni(n,γ)	4.0%	2.3%	9.5%	9.5%	4.5% (39.9 mb)	3.9% (38.7 mb)
(n,el)	1.6%	1.6%				

a) See Table 3.5 for explanation of differences between this work and Atlas.
b) Computed by NJOY using MF33 grid in GROUPR.
c) Computed by NJOY using MF33 grid. Cross sections refer to ENDF/B-VII.0.
$^{+)}$ No value is given in Atlas; estimated by PO in July 2010.

Overall, our final results represent improvement over initial results in two respects:

- Excellent agreement with uncertainties of capture resonance integrals given in Atlas was achieved for all three major structural materials.
- Data of primary interest for AFCI applications, elastic scattering cross section uncertainties at energies above about few hundred keV, were reduced

compared to our initial values. We believe that plausible values of uncertainties were reached at these energies, ~12% for ^{52}Cr, 7-8% for ^{56}Fe and 5-6% for ^{58}Ni.

Chapter 7

Conclusions

We evaluated covariances for neutron capture and elastic scattering cross sections on ^{52}Cr, ^{56}Fe and ^{58}Ni in the resonance region which extends beyond 800 keV for each of them. Use was made of the recently developed covariance formalism based on kernel approximation along with data in the Atlas of Neutron Resonances. Covariances in the thermal region were directly deduced from experimental data and thus treated independently from the resonance region. Our results are stored in file MF33 and should serve as covariances of cross sections in ENDF/B-VII.0 library. Processed 33-group data should be adopted by AFCI-2.0 covariance library.

Kernel approximation works very well for capture as demonstrated by ^{52}Cr, ^{56}Fe as well as ^{58}Ni. These materials are almost pure scatterers, meaning that neutron widths are much larger than radiative widths, $\Gamma_n >> \Gamma_\gamma$. As a consequence, $\Gamma_n/\Gamma \approx 1$ and therefore capture covariances are essentially determined by radiative width uncertainties, $\Delta\Gamma_\gamma$. We note, however, that they strongly depend on correlations between radiative widths of different resonances, corr($\Gamma_\gamma, \Gamma_\gamma$), which are unknown and had to be estimated. At energies above several hundreds keV our uncertainties for capture cross sections are in the range of 25-30%. These uncertainties are consistent with low values of related capture cross sections which are below 10 mb.

Kernel approximation for elastic scattering represents less robust approach. This is mostly due to interference effects which we handle fairly roughly by resorting to broad energy bins in which negative and positive interferences approximately compensate. Specific challenge for ^{52}Cr, ^{56}Fe and ^{58}Ni is caused by high

energy resonances which prevent the use of low energy approximation. Despite these difficulties we have shown that elastic cross sections at high resonance energies are dominated by potential scattering. Therefore, at these high energies elastic scattering covariances are largely determined by scattering radius uncertainty, $\Delta R'$. As a consequence, at energies above several hundreds keV elastic scattering cross section uncertainties are in the range of about 10%. Overall, our results for elastic scattering cross section covariances should be viewed as reasonable estimates. They are relatively insensitive to adopted values of correlation coefficients between neutron widths of individual resonances, corr(Γ_n, Γ_n) and between scattering radius and neutron width, corr(R',Γ_n), which are unknown and had to be estimated.

Comparison with ENDF/A evaluations performed by the ORNL group using the code SAMMY was done for ^{52}Cr and ^{58}Ni. Some considerable differences with our results were observed and at least partially explained by the lack of correlations and neglect of $\Delta R'$ contribution in ENDF/A evaluations.

Our results were subject to QA checks, including compliance with ENDF-6 formatting, mathematical properties of covariance matrices and limited uncertainty testing. Uncertainties were tested against available integral quantities with good outcome, and also against 2% minimal value.

Acknowledgment

This work has been performed under AFCI covariance data project sponsored by DOE-NE as well as under ARRA project of developing neutron cross section covariances for ENDF/B-VII library sponsored by DOE-SC. This sponsorship is gratefully acknowledged.

One of us (YSC) is grateful to the NNDC for warm hospitality during his sabbatical leave of absence from KAERI. The authors are grateful to Mike Herman and Marco Pigni for numerous discussions on covariances. They wish to thank Ramon Arcilla and Andrej Trkov for assistance and advice on processing.

Bibliography

[1] P. Obložinský, Y.-S. Cho, C. Mattoon, S.F. Mughabghab, "Formalism for neutron cross section covariances in the resonance region using kernel approximation", Brookhaven National Laboratory, Report BNL-91287-2010 (April 2010).

[2] P. Obložinský, C. Mattoon, M. Herman, S.F. Mughabghab, M. Pigni, P. Talou, G. Hale, A.C. Kahler, T. Kawano, R. Little, P. Young, "Progress on Nuclear Data Covariances: AFCI-1.2 Covariance Library", Brookhaven National Laboratory, Report BNL-90897-2009 (September 2009).

[3] M.B. Chadwick, P. Obložinský, M. Herman *et al*, "ENDF/B-VII.0: Next Generation of Evaluated Nuclear Data Library for Nuclear Science and Technology", Nuclear Data Sheets **107** (2006) 2931.

[4] S.F. Mughabghab, "Atlas of Neutron Resonances: Thermal Cross Sections and Resonance Parameters", Elsevier Publisher, Amsterdam, 2006.

[5] M. Herman and A. Trkov (editors), "ENDF-6 Formats Manual: Data Formats and Procedures for the Evaluated Nuclear Data File ENDF/B-VI and ENDF/B-VII", Brookhaven National Laboratory, Report BNL-90365-2009 (CSEWG Document ENDF-102), June 2009, p. 317.

[6] L. Leal, H. Derrien, K. Guber, G. Arbanas and D. Wiarda, "^{52}Cr ORNL Resonance Evaluation Including Covariance", September 2009, retrieved from ENDF/A in May 2010.

[7] L. Leal, H. Derrien, K. Guber, G. Arbanas and D. Wiarda, "^{53}Cr ORNL Resonance Evaluation Including Covariance", September 2009, retrieved from ENDF/A in May 2010.

[8] P. Pereslavtsev, A. Konobeyev and U. Fischer, "^{52}Cr+n High Energy Evaluation", September 2009, retrieved from ENDF/A in May 2010.

[9] H. Derrien, L. Leal, N.M. Larson, D. Wiarda, K. Guber and G. Arbanas, "Evaluation of the Resonance Parameters of ^{55}Mn in the Energy Range 0 to 122 keV", September 2009, retrieved from ENDF/A in May 2010.

[10] H. Derrien, L. Leal, K. Guber, D. Wiarda and G. Arbanas, "Reevaluation of ^{58}Ni Resonance Parameters in the Energy Range Thermal to 812 keV", July 2009, retrieved from ENDF/A in May 2010.

[11] H. Derrien, L. Leal, K. Guber, D. Wiarda and G. Arbanas, "Reevaluation of ^{60}Ni Resonance Parameters in the Energy Range Thermal to 810 keV", July 2009, retrieved from ENDF/A in May 2010.

[12] K. Shibata, O. Iwamoto, T. Nakagawa *et al*, "JENDL-4.0: A New Library for Nuclear Science and Technology", J. Nucl. Sci. Technol., to be published.

[13] "KADoNiS, Karlsruhe Astrophysical Database of Nucleosynthesis in Stars", www.kadonis.org, data retrieved in June 2010.

[14] M.T. Pigni, F.S. Dietrich, M. Herman and P. Obložinský, "Optical model and cross-section uncertainties", manuscript of the paper, 2010.

[15] R. Capote *et al*, "RIPL - Reference Input Parameter Library for Calculations of Nuclear Reactions and Nuclear Data Evaluations", Nuclear Data Sheets **110** (2009) pp. 3107-3214.